Water-soluble brown carbon in atmospheric aerosols along the transport pathway of Asian dust: Optical properties, chemical compositions, and potential sources

Hui Wen [a,b], Yue Zhou [a], Xuanye Xu [c], Tianshuang Wang [a], Quanliang Chen [c], Qingcai Chen [d], Weijun Li [e], Zhe Wang [f], Zhongwei Huang [a], Tian Zhou [a], Jinsen Shi [a], Jianrong Bi [a], Mingxia Ji [a], Xin Wang [a,b,*]

[a] Key Laboratory for Semi-Arid Climate Change of the Ministry of Education, College of Atmospheric Sciences, Lanzhou University, Lanzhou 730000, China
[b] Institute of Surface-Earth System Science, School of Earth System Science, Tianjin University, Tianjin 300072, China
[c] College of Atmospheric Sciences, Chengdu University of Information Technology, Chengdu 610225, China
[d] School of Environmental Science and Engineering, Shaanxi University of Science and Technology, Xi'an 710021, China
[e] Department of Atmospheric Sciences, School of Earth Sciences, Zhejiang University, Hangzhou 320007, China
[f] Division of Environment and Sustainability, The Hong Kong University of Science and Technology, Hong Kong, China

HIGHLIGHTS

- Light-absorbing and fluorescence properties of atmospheric WS-BrC in the remote, rural, and urban areas along the transport pathway of Asian dust were described.
- Organic compounds in dust plume from the Gobi Desert are important sources of WS-BrC, especially for remote area.
- Atmospheric aging processes may modify the light-absorbing and fluorescence properties of WS-BrC.
- WS-BrC is an important contributor of light-absorbing aerosol especially at shorter wavelengths in northern China.

GRAPHICAL ABSTRACT
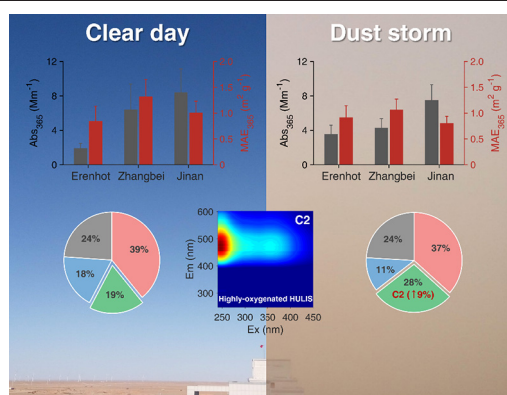
ARTICLE INFO

ABSTRACT

As an important type of light-absorbing aerosol, brown carbon (BrC) has the potential to affect the atmospheric photochemistry and Earth's energy budget. A comprehensive field campaign was carried out along the transport pathway of Asian dust during the spring of 2016, including a desert site (Erenhot), a rural site (Zhangbei), and an urban site (Jinan), in northern China. Optical properties, bulk chemical compositions, and potential sources of water-soluble brown carbon (WS-BrC) were investigated in atmospheric total suspended particulate (TSP) samples. Samples from Zhangbei had higher mass absorption efficiency at 365 nm (MAE_{365}, $1.32 \pm 0.34\ m^2\ g^{-1}$) than those from Jinan ($1.00 \pm 0.23\ m^2\ g^{-1}$) and Erenhot ($0.84 \pm 0.30\ m^2\ g^{-1}$). Compere to the non-dust samples, elevated water-soluble organic carbon (WSOC) concentrations and MAE_{365} values of dust samples from Erenhot are related to the input of high molecular weight organic compounds and biogenic matter from the Gobi Desert, while lower values from Zhangbei and Jinan are attributed to the dilution effect caused by strong northwesterly winds. Based on fluorescence excitation–emission matrix spectra and parallel factor analysis, two humic-like (C1 and C2) and two protein-like (C3 and C4) substances were identified. Together, C1 and C2 accounted for ~64% of total fluorescence intensity at the highly polluted urban Jinan site; C3 represented ~45% at the rural Zhangbei site

* Corresponding author at: Key Laboratory for Semi-Arid Climate Change of the Ministry of Education, College of Atmospheric Sciences, Lanzhou University, Lanzhou 730000, China & Institute of Surface-Earth System Science, School of Earth System Science, Tianjin University, Tianjin 300072, China
   E-mail address: wxin@lzu.edu.cn (X. Wang).

Source apportionment
Radiative forcing efficiency

where local biomass burning affects; and C4 contributed ~24% in the desert region (Erenhot) due to dust-sourced biogenic substances. The relative absorptive forcing of WS-BrC compared to black carbon at 300–400 nm was about 31.3%, 13.9%, and 9.2% during non-dust periods at Erenhot, Zhangbei, and Jinan, respectively, highlighting that WS-BrC may significantly affect the radiative balance of Earth's climate system and should be included in radiative forcing models.

1. Introduction

Carbonaceous aerosols, including black carbon (BC) and organic carbon (OC), may significantly affect Earth's radiative balance and global climate change (IPCC, 2013). BC has been recognized as an efficient absorber of solar radiation (Bond and Bergstrom, 2006). The direct radiative forcing of BC has been estimated as $+0.88$ W m^{-2} with an uncertainty range of $+0.17$ to $+1.48$ W m^{-2} (Bond et al., 2013). OC was initially assumed to be an efficient light-scattering species with invariant optical properties in some global climate models (Chen and Bond, 2010; Laskin et al., 2015). However, there is increasing evidence from laboratory and field studies that a significant portion of OC with brownish to yellowish color (termed "brown carbon", BrC) also has light-absorbing properties and potentially contribute to direct positive climate forcing (Andreae and Gelencsér, 2006; Saleh et al., 2013). Another concern over atmospheric BrC is that it tends to absorb more solar radiation in the near-ultraviolet (UV) and visible (Vis) spectral ranges, indirectly influencing tropospheric photochemical processes (Laskin et al., 2015). Modeling has shown that BrC contributes to 7%–19% of the total atmospheric radiative forcing on a global scale (Feng et al., 2013). The radiative contribution of BrC may be more significant over East and South Asia where its atmospheric concentrations are higher (Gustafsson et al., 2009; Cheng et al., 2011; Dasari et al., 2019). However, there is still great uncertainty concerning the radiative effects of BrC in current climate models, as its optical properties are not fully constrained, due mainly to its complex chemical composition and emission sources, and its evolution under different and variable atmospheric conditions (Zhang et al., 2013; Kim et al., 2016). BrC forms as primary aerosols through biomass burning, fossil fuel combustion, biological and soil humic emissions; or as secondary aerosols derived from anthropogenic and biogenic volatile organic compounds via homogenous/heterogeneous oxidation and gas–particle conversions (Andreae and Gelencsér, 2006; Chen and Bond, 2010; Lin et al., 2015). However, relationships between BrC absorption and its different sources are still unclear and require further investigation (Saleh, 2020).

Asian dust storms, occurring frequently in spring and early summer, arise mainly from arid and semi-arid areas of Mongolia and northern and northwestern China (Duce et al., 1980; Garrison et al., 2003; Huang et al., 2014). Prevailing westerly winds carry the dust plumes through East Asia (Wang et al., 2009a) and across the North Pacific Ocean (Huang et al., 2008) to North America (Husar et al., 2001) and the Arctic (Huang et al., 2015), and even more than one full global circuit in 13 days (Uno et al., 2009). The estimated annual flux of Asian dust is 800 Tg yr^{-1} (Huang et al., 2014). Chen et al. (2017) reported that the Gobi Desert, rather than the Taklimakan Desert, contributes most to atmospheric dust concentrations in East Asia with ~35% being transported downwind in spring. Deposited mineral dust particles provide micronutrients such as Fe for marine ecosystems and stimulate phytoplankton productivity (Garrison et al., 2003). Dust plumes are also an important vector for long-range transport of organic matter, especially for alpine and other remote regions (Mladenov et al., 2011b; Wang et al., 2012; Xie et al., 2016). Organic constituents of desert dust aerosol include plant debris, bacteria, archaea, and fungal spore (Tang et al., 2018). During long-range transport, dust particles can mix with inorganic and organic species such as sulfate, nitrate, ammonium, dicarboxylic acid, and volatile phenols with consequent changes to their chemical, optical, and hygroscopic properties (Wang et al., 2014; Tang et al., 2016). Transition metals such as Fe(III) in dust catalyze polymerization reactions of atmospheric phenols, providing an efficient pathway for secondary BrC formation (Slikboer et al., 2015; Lavi et al., 2017). The investigation of chemical characteristics and associated optical properties of organic matter in Asian dust and its influence on downwind regions is thus crucial in assessing the impacts of Asian dust on regional and global scales (Tobo et al., 2010).

Fluorescence excitation–emission matrix (EEM) spectroscopy is a sensitive and rapid method for providing chemical and structural information on chromophores, and has been widely applied in characterizing chemical properties of dissolved organic matter in terrestrial and aquatic ecosystems including soils, rivers, and oceans (Coble, 1996; Stedmon and Markager, 2005; Ohno et al., 2008; Birdwell and Engel, 2010). It is increasingly used to explore types, sources, and transformation mechanisms of atmospheric BrC in both laboratory and field studies (Lee et al., 2014; Aiona et al., 2017; Fan et al., 2020). Although fluorescent components distinguished by parallel factor (PARAFAC) analysis are well-characterized in terrestrial and aquatic systems, the technique might not be straightforward with atmospheric BrC because its sources, physicochemical processes, and transformation pathways are very different (Chen et al., 2016a; Wang et al., 2020). The greatest challenge in applying EEM–PARAFAC method to atmospheric BrC is the lack of a well-established classification system for fluorescence spectra. Despite recent progress in BrC characterization by this method for highly polluted urban aerosols (Yan and Kim, 2017; Wang et al., 2020), knowledge of fluorescence characteristics of rural and remote aerosols is lacking due to the limited observations undertaken to date (Xie et al., 2016; Wu et al., 2019b), especially for dust source regions such as the Gobi Desert. More field studies are urgently needed to investigate the fluorescence properties of atmospheric BrC in typical remote, rural, and urban areas.

To address these shortfalls, a comprehensive campaign was undertaken at three sites along the transport pathway of Asian dust, namely Erenhot (desert), Zhangbei (rural), and Jinan (urban), northern China, during the spring of 2016. Light-absorbing and fluorescence properties, bulk chemical compositions of water-soluble BrC (WS-BrC) were investigated using UV–Vis absorption spectrophotometry, EEM, and thermo-derived carbonaceous and inorganic ion analyses, with the aim of providing useful information on the optical and chemical properties of different types of organic aerosol (OA) in northern China.

2. Methodology

2.1. Sampling sites

Erenhot lies in the eastern part of the Gobi Desert, suffering frequent and severe dust events (Fig. 1) especially in spring and early summer due to low precipitation (annual precipitation ~150 mm), sparse vegetation, and frequent cyclonic activity (Qian et al., 2002). The Erenhot sampling site (43.67°N, 111.95°E; 957 m above sea level, a.s.l.) is on the northwestern fringe of Erenhot city, on a rooftop ~20 m above ground level (a.g.l.). Erenhot has a low population density, with no obvious anthropogenic pollution sources near the sampling site.

Zhangbei is a town north of Zhangjiakou city. The sampling site (41.16°N, 114.70°E; 1395 m a.s.l.) is in a rural area, on top of a container
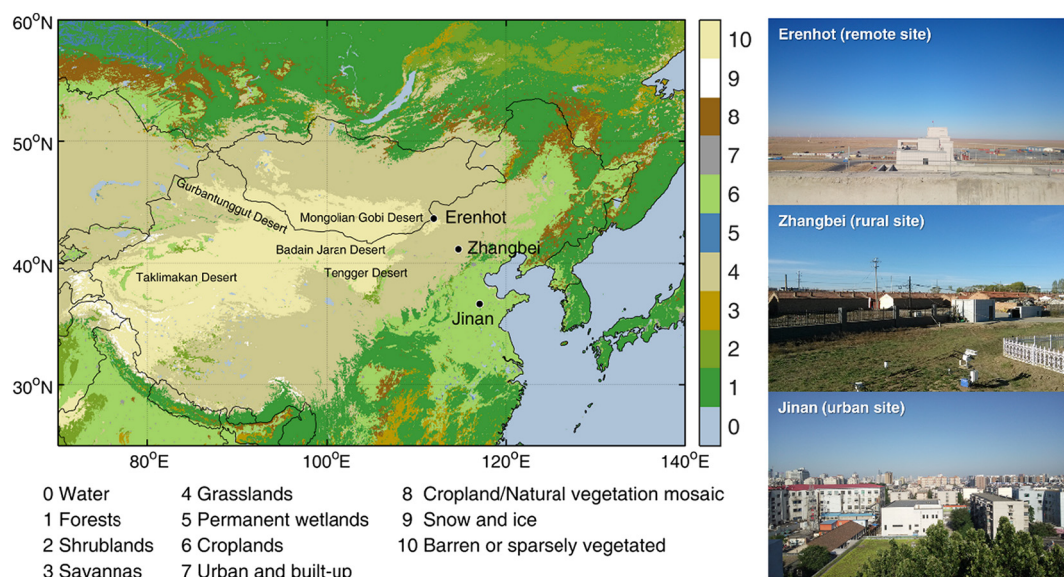
Fig. 1. Land cover map of the study area and the sampling locations. The classification of surface vegetation types, based on the MODIS global land cover type product (MCD12C1; http://ladsweb.nascom.nasa.gov), indicates barren or sparsely vegetated at Erenhot, grassland at Zhangbei, and cropland at Jinan. Photographs taken from the sampling sites are shown at right panel.

at the Zhangbei Meteorological Bureau (~4 m a.g.l.) and ~ 3 km west of the local town center, surrounded by low-rise residential houses and farmland (Fig. 1). This area lies at the junction of the Inner Mongolia Plateau and the North China Plain (NCP). The surface is generally covered by grass but has undergone severe steppe desertification in past decades due to intensified human activities such as extensive cultivation and overgrazing.

Jinan is the capital of Shandong Province and is a highly industrialized and populated city in the eastern NCP, suffering severe air pollution due to SO_2, NO_x, and particulate matter released mainly by coal-fired power plants, industry activities, and vehicles (Yang et al., 2012). The sampling site there (36.67°N, 117.06°E; 48 m a.s.l.) was on a rooftop (~25 m a.g.l.) in the central campus of Shandong University. There are two heavy traffic roads around this site: the East 2nd Ring Road (~900 m to the east) and the Shanda Road (~600 m to the west), but no significant industrial activity in the vicinity.

2.2. Sample collection

Total suspended particulate (TSP) samples were collected simultaneously at the three sites by mid-volume aerosol samplers (model TH-150C III, Tianhong Ltd., Wuhan, China) at a flow rate of 100 L min^{-1} from 08:00 a.m. to 05:00 a.m. the next day (Beijing time). Samples were collected on quartz microfiber filters (Φ 90 mm; QM-A, Whatman, Maidstone, UK) pre-baked at 450 °C for 6 h to remove residual organics. During the sampling period from March 25 to May 31, 2016, a total of 55, 59, and 60 valid TSP samples were collected at Erenhot, Zhangbei, and Jinan, respectively. After collection, the samples were individually sealed and preserved in darkness at −20 °C for subsequent analysis. Filters were weighted at least three times before and after sampling, using an electronic analytical balance (model BSA124S, Sartorius, Göttingen, Germany) after 24-h stabilization under constant temperature (20 ± 1 °C) and relative humidity (40% ± 2%).

2.3. Instrumental analyses

2.3.1. Thermal/optical carbon analysis

A circular subsample (0.296 cm^2) was punched from each filter to determine the contents of four organic carbon (OC) fractions (OC1, OC2, OC3, and OC4), three elemental carbon (EC) fractions (EC1, EC2,

and EC3), and pyrolyzed organic carbon (OPC) using a carbon analyzer (DRI model 2001A, Atmoslytic Inc., Calabasas, CA, USA) following IMPROVE_A temperature protocol with thermal–optical reflectance corrections; details can be found elsewhere (Chow et al., 2007). To eliminate carbonate carbon which may interfere with carbon determinations, samples collected during dust events were acidified with HCl before analysis (Chow and Watson, 2002; Mladenov et al., 2011a). The detection limit for the carbon analyzer was 0.20 μg C cm^{-2}. All data reported here were corrected by filter blanks.

2.3.2. Water-soluble inorganic ions and WSOC analyses

For water-soluble inorganic ions analysis, a 2.0 cm^2 filter punch from each sample was ultrasonically extracted with 20 mL ultrapure water (resistivity: 18.2 MΩ cm) in a polypropylene vial for 30 min. Extracts were filtered through polytetrafluoroethylene (PTFE) syringe filters (Jinteng Ltd., Tianjin, China) of 0.22 μm pore size to remove particles and filter debris. Three anions (Cl^-, SO_4^{2-}, and NO_3^-) and five cations (Na^+, NH_4^+, K^+, Mg^{2+}, and Ca^{2+}) were determined by an ion chromatograph (model Dionex 600, Thermo Scientific, Waltham, MA, USA) using IonPac AS22 and CS12A analytical columns, respectively. The detection limit was 0.05 mg L^{-1} for all ions.

For WSOC and spectroscopic analyses, a filter punch (3.14 cm^2) was extracted similarly in a pre-baked glass vial. Water-soluble organic carbon (WSOC) in the filtrates were quantified with a total organic carbon (TOC) analyzer (model Aurora 1030 W, OI Analytical, College Station, TX, USA). Triplicate analyses were performed and average values (after blank corrected) were reported. The detection limit was 2 ppb, and the average relative standard deviation of measurements was ~1%.

2.3.3. UV–Vis absorption and EEM fluorescence spectra

The UV–Vis absorption spectra and EEM fluorescence spectra were measured simultaneously using an Aqualog spectrofluorometer (Horiba Scientific, Edison, NJ, USA) equipped with a 1 cm quartz cuvette. The UV–Vis absorption spectra were measured at wavelengths of 240–600 nm with intervals of 5 nm and were the same for EEM excitation wavelengths (λ_{Ex}); the emission wavelengths (λ_{Em}) were set to 247.84–825.46 nm with 4.65 nm intervals. The integration time was 0.3 s. To reduce the inner filter effect (IFE) in EEM measurement, absorbances at 250 nm were controlled within 0.5 AU (arbitrary unit) for all samples (Chen et al., 2019; Kothawala et al., 2013). Ultrapure water was

analyzed as a blank reference and for baseline correction before sample analysis.

2.4. Data analyses

2.4.1. UV–Vis absorption spectra

The absorbance at 600 nm (A_{600}) was subtracted from all spectral data to correct for scattering effects and baseline shifts during measurement, and absorbances at a given wavelength (A_λ) were converted to the light absorption coefficient (Abs_λ, Mm^{-1}) using the following equation (Hecobian et al., 2010):

$$Abs_\lambda = (A_\lambda - A_{600}) \frac{V_l}{V_a \cdot l} \cdot \ln(10), \tag{1}$$

where V_l is the volume of ultrapure water used in the extraction (9 mL); V_a (m^3) is the volume of sampled air through the filter punch (3.14 cm^2); l is the cuvette path length (0.01 m); and $\ln(10)$ converts from base-10 to natural logarithm. The mass absorption efficiency (MAE_λ, $m^2\ g^{-1}$) is defined as the measured Abs_λ divided by the mass concentration of WSOC (C_{WSOC}, $\mu g\ m^{-3}$), expressed as follows:

$$MAE_\lambda = \frac{Abs_\lambda}{C_{WSOC}}. \tag{2}$$

To characterize the light-absorbing properties of WS-BrC, the specific absorbance and MAE are usually calculated at 365 nm (the average of 360 and 370 nm) to avoid interference from other non-organic compounds (e.g., nitrate) (Hecobian et al., 2010). Note that WS-BrC in this study is an ensemble of hydrophilic organic compounds absorbing solar radiation efficiently in the near-UV and visible ranges. The spectral dependence of light absorption was investigated by calculation of the absorption Ångström exponent (AAE) by a linear regression fit at wavelengths of 300–400 nm (Park and Yu, 2016):

$$AAE = \frac{-\ln(A(\lambda_1)/A(\lambda_2))}{\ln(\lambda_1/\lambda_2)}. \tag{3}$$

2.4.2. EEM–PARAFAC analysis

Before performing the PARAFAC steps using drEEM toolbox (version 0.2.0; Murphy et al., 2013), the raw EEMs ($n = 174$) were corrected for background signals, spectral bias, IFEs, and converted to Raman units (RU). Several tests for two- to twelve- components models were performed (Fig. S1), and only four-component model was validated for all comparisons with $S_4C_6T_3$ split scheme (Fig. S2). The maximum fluorescence intensity of each component (F_{max}) was calculated (Murphy et al., 2013). More details of PARAFAC analysis are given in Supplementary Text S1.

2.4.3. Fluorescence quantum yields

Fluorescence quantum yield is defined as the ratio of fluorescent photon number emitted by the chromophore to the absorbed photon number, and is affected mainly by the chemical structure and properties of the compound concerned (Lee et al., 2013). The apparent fluorescence quantum yields (AQY) of aerosol samples can be estimated using the following equation (Xiao et al., 2018):

$$AQY_\lambda = \frac{\int_{Em} F(\lambda_{Ex}\lambda_{Em}) d\lambda_{Em}}{A(\lambda_{Ex}) \int_{Em} d\lambda_{Em}} \bigg|_{Ex}, \tag{4}$$

where F represents the fluorescence intensity (in RU) at each excitation (240–450 nm) and emission (247–600 nm) wavelength.

2.4.4. Direct solar absorption of BrC relative to EC

EC is a well-established proxy for black carbon (BC), which is known as the most efficient light-absorbing carbonaceous species in the atmosphere (Bond and Bergstrom, 2006). Solar energy absorbed by WS-BrC (E_{WS-BrC}) and BC (E_{BC}) at ground level was estimated using Eqs. (5) and (6), respectively (Kirillova et al., 2014):

$$E_{WS-BrC} = \int I_0(\lambda) \left\{ 1 - e^{-\left(MAC_{WS-BrC} \times \left(\frac{\lambda_0}{\lambda}\right)^{AAE_{WS-BrC}} \times C_{WSOC} \times h_{ABL} \right)} \right\} d\lambda, \tag{5}$$

$$E_{BC} = \int I_0(\lambda) \left\{ 1 - e^{-\left(MAC_{BC} \times \left(\frac{\lambda_0}{\lambda}\right)^{AAE_{BC}} \times C_{EC} \times h_{ABL} \right)} \right\} d\lambda, \tag{6}$$

where C_{EC} is the mass concentration of EC ($\mu g\ m^{-3}$) based on the measurement data; $I_0(\lambda)$ is the solar irradiance from ASTM G173–03 reference spectra (Chen and Bond, 2010); MAC_{WS-BrC} and MAC_{EC} are the mass absorption cross-section for particulate BrC (converted from MAE of bulk aqueous extracts; see Text S2) and EC, respectively, and the corresponding reference wavelength (λ_0) was 365 nm and 550 nm (Bosch et al., 2014). For the current simplistic model, MAC_{EC} and AAE_{EC} were set to 7.5 ± 1.2 $m^2\ g^{-1}$ and 1 for uncoated EC particles, respectively (Bond and Bergstrom, 2006). h_{ABL} is the vertical height of the aerosol boundary layer (1000 m). Assumptions pertaining to simplistic estimate have been described elsewhere (Bosch et al., 2014; Kirillova et al., 2014). Fractions (f, in %) of solar energy absorbed by WS-BrC relative to EC were calculated by numerical integration of E_{WS-BrC} and E_{EC}.

2.4.5. Simple forcing efficiency

The simple forcing efficiency (SFE) method (Bond and Bergstrom, 2006) was used to estimate first-order clear-sky direct radiative effects caused by WS-BrC. The SFE ($W\ g^{-1}$) represents the energy added to the atmosphere by a given mass of particles (Laskin et al., 2015). Here, we focused on the light absorption effect of WS-BrC without considering its scattering effect, with the absorption part of wavelength-dependent SFE of WS-BrC (SFE_{abs}) being described as (Bikkina and Sarin, 2019):

$$\frac{dSFE_{abs}}{d\lambda} = D \frac{dS(\lambda)}{d\lambda} \tau_{atm}^2 (1 - F_c) \times 2\alpha_s \times MAC_{WS-BrC}(\lambda), \tag{7}$$

where S and τ_{atm} refer to solar irradiance and atmospheric transmission, respectively, with both being from ASTM G173–03 reference spectra. D is the daytime fraction (0.5), F_c is the cloud fraction (0.6), and α_s is the surface albedo (0.19 for Earth average) (Chen and Bond, 2010). Net forcing was calculated by integrating SFE_{abs} values. More details of the calculation are provided in Text S2.

3. Results and discussion

3.1. Variations of TSP and carbonaceous components

Throughout the 2016 campaign, we identified 21 dust samples at the Erenhot site, 6 at the Zhangbei site, and 2 at the Jinan site, based on daily TSP concentrations, surface meteorological parameters (ambient temperature, pressure, relative humidity, visibility, wind direction, and wind speed from the China Meteorological Administration, as shown in Fig. S3), and manual weather records. Meteorological parameters at Zhangbei were also monitored by an automatic meteorological station (model WXT520, Vaisala Inc., Helsinki, Finland) at 5 min intervals. Daily variations of TSP and carbonaceous compositions at the three sampling sites are illustrated in Fig. 2, and the concentrations of chemical compositions during dust and non-dust periods are summarized in Table 1.

Meteorological records indicate that the remote Erenhot site was generally clear with high visibility (>25 km) and low TSP concentrations (88.3 ± 47.4 $\mu g\ m^{-3}$; arithmetic mean ± standard deviation) except during dust periods. Atmospheric EC is derived mainly from incomplete combustion of fossil fuels and biomass (Bond and
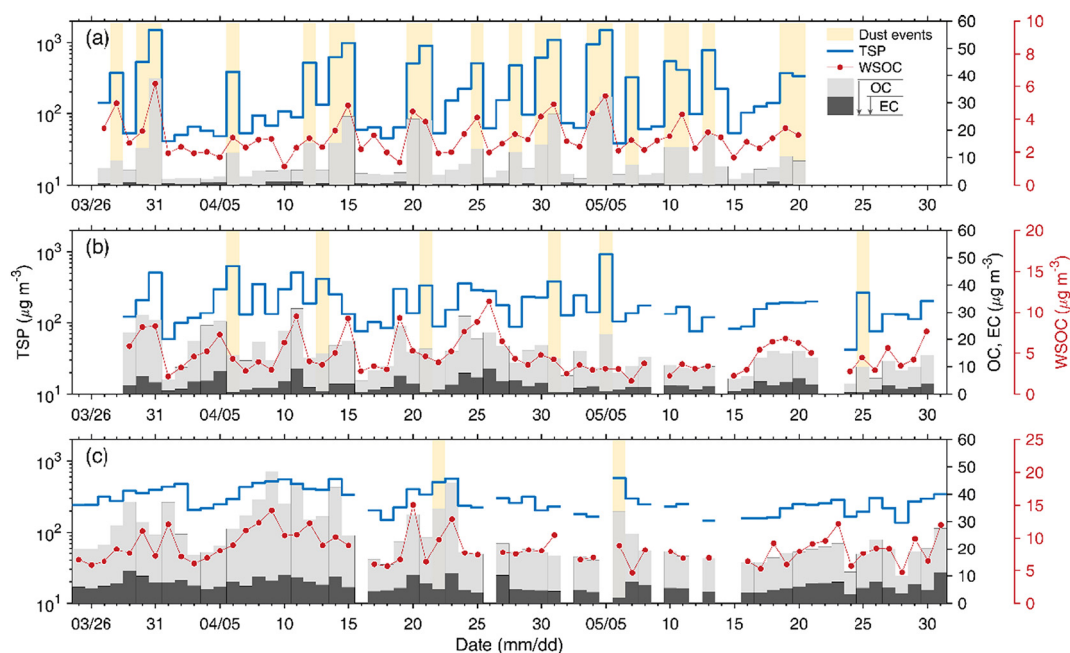
Fig. 2. Temporal variations of TSP, OC, EC, and WSOC concentrations (μg m^{-3}) for (a) Erenhot, (b) Zhangbei, and (c) Jinan sites during the entire sampling period. Dust episodes are highlighted by yellow shading. Gaps in the series were due to adverse weather conditions (e.g., rainy days) or instrument failure.

Bergstrom, 2006) and is commonly treated as an unambiguous tracer of primary combustion emissions (Chow et al., 2004). Low EC concentrations (0.60 ± 0.32 μg m^{-3}) at Erenhot indicate a negligible impact of combustion activities there. In contrast, high TSP concentrations were observed at the urban Jinan site (294.5 ± 113.1 μg m^{-3}), with almost half of the samples exceeding the Chinese Ambient Air Quality Standards (CAAQS, GB3095–2012) Grade II pollutant concentration limit (300 μg m^{-3}). Maximum recorded OC and EC concentrations at Jinan were 48.33 and 11.97 μg m^{-3}, respectively, indicating the high intensity of air pollutant emission in the densely populated area. An intermediate TSP level was observed at the rural Zhangbei site (177.4 ± 101.6 μg m^{-3}), with OC and EC concentrations of 14.85 ± 3.63 and 3.63 ± 2.22 μg m^{-3}, respectively, which were about half of those measured at Jinan.

Atmospheric WSOC, typically accounting for 20–80% of particulate OC, plays an important role in hygroscopicity, cloud nucleating, and optical properties of aerosols (Xie et al., 2016). The abundance of WSOC exhibited trends similar to that of OC at the three sites (Fig. 2). WSOC concentrations averaged 2.31 ± 0.50, 4.92 ± 2.23, and 8.40 ± 2.39 μg m^{-3} at Erenhot, Zhangbei, and Jinan, respectively. WSOC generally comprises oxygenated organic compounds such as carboxylic acids,

aldehydes, ketones, and alcohols (Pathak et al., 2011). Most OC emitted directly from primary sources (POC) such as combustion, industrial, and traffic activities are water-insoluble (Kumagai et al., 2009). However, as POC diffuses away from its source and reacts with oxidants in the atmosphere, it may gradually be oxidized to compounds containing more polar functional groups, thus becoming more water-soluble (Decesari et al., 2002; Pathak et al., 2011). The water-soluble fraction of total OC (WSOC/OC) can therefore be used as an indicator of the degree of oxidation of aerosols (Kumagai et al., 2009; Ram et al., 2012). High WSOC/OC ratios measured at Erenhot (0.57 ± 0.18) are consistent with those observed at a remote site on the southeastern Tibetan Plateau (0.51 ± 0.18; Wu et al., 2019a), while ratios at Zhangbei (0.35 ± 0.10) and Jinan (0.37 ± 0.09) were relatively low and more similar to those measured in megacities such as Shanghai (0.35 ± 0.1) and Guangzhou (0.32 ± 0.1), China (Pathak et al., 2011).

The most severe dust storm event during the study occurred on 5–6 May 2016, with extremely high TSP concentrations of 1488.7, 920.2, and 574.0 μg m^{-3} along the Erenhot-Zhangbei-Jinan transport route, respectively. True color images from MODIS (MODerate-resolution Imaging Spectroradiometer, https://worldview.earthdata.nasa.gov) verified that the dust plume originating in the Gobi Desert was transported

Table 1
Average concentrations of TSP, carbonaceous species, and main water-soluble inorganic ions (μg m^{-3}) during dust and non-dust periods of the three sampling sites. Results are given as arithmetic mean ± standard deviation.

Site	Erenhot		Zhangbei		Jinan	
	Non-dust (n = 34)	Dust (n = 21)	Non-dust (n = 53)	Dust (n = 6)	Non-dust (n = 58)	Dust (n = 2)
TSP	88.3 ± 47.4	680.2 ± 351.9	177.4 ± 101.6	493.3 ± 242.2	294.5 ± 113.1	538.1 ± 50.7
OC	4.42 ± 1.43	17.78 ± 8.36	14.85 ± 3.63	15.45 ± 4.32	23.67 ± 8.62	34.27 ± 0.72
EC	0.60 ± 0.32	0.07 ± 0.12	3.63 ± 2.22	0.39 ± 0.22	6.63 ± 2.17	3.59 ± 2.16
WSOC	2.31 ± 0.50	3.91 ± 0.96	4.92 ± 2.23	4.03 ± 0.58	8.40 ± 2.39	9.32 ± 0.64
WSOC/OC	0.57 ± 0.18	0.25 ± 0.10	0.35 ± 0.10	0.28 ± 0.10	0.37 ± 0.09	0.27 ± 0.01
nss-ndust-K$^+$	0.11 ± 0.09	–	0.73 ± 0.53	–	0.46 ± 0.32	–
Ca^{2+}	1.98 ± 1.07	10.11 ± 4.53	5.67 ± 3.72	8.93 ± 3.72	16.00 ± 4.61	17.02 ± 2.00
SO$_4^{2-}$	1.59 ± 0.82	3.42 ± 1.52	5.53 ± 4.73	3.64 ± 1.48	16.99 ± 10.22	7.67 ± 4.30
NO$_3^-$	0.91 ± 0.57	1.41 ± 0.80	6.53 ± 6.24	1.63 ± 0.93	20.21 ± 13.89	8.80 ± 2.08

eastward, affecting most cities in the NCP (Fig. S4) and reaching Japan (Nishita-Hara et al., 2019). At Erenhot, local visibility decreased to <50 m during the dust storm with wind speeds exceeding 15 m s^{-1} (Figs. S3 and S5). TSP concentrations increased markedly, with an average value (680.2 $\pm$ 351.9 μg m^{-3}) approximately eight times that of non-event days. OC and WSOC concentrations surged to 17.78 $\pm$ 8.36 μg m^{-3} and 3.91 $\pm$ 0.96 μg m^{-3}, respectively, demonstrating that dust deposition is an important source of organic matter in such remote region. Wang et al. (2013) attributed the increase in OC during dust storms to the input of biogenic organics (e.g., bacteria, fungal spores, plant pollen and debris) carried by sand and dust particles from desert regions. Water-soluble organic compounds such as glucose (Wang et al., 2009b), trehalose (Simoneit et al., 2004), and humic acid (Alexander et al., 2015) are enriched in natural dust particles, and may be associated with peaks in WSOC during dust periods. In contrast, EC decreased substantially to below the detection limit of the carbon analyzer (0.07 $\pm$ 0.12 μg m^{-3}), indicating that dust samples collected at Erenhot were unaffected by anthropogenic pollution, and rather represent natural dust of the Gobi Desert. Dust plumes gradually diminished after long-range downwind transport, with lower TSP loadings of 493.3 $\pm$ 242.2 and 538.1 $\pm$ 50.7 μg m^{-3} at Zhangbei and Jinan, respectively. Compared to non-event days, relatively low EC values were measured in dust samples from Zhangbei (0.39 $\pm$ 0.22 μg m^{-3}) and Jinan (3.59 $\pm$ 2.16 μg m^{-3}) (Fig. 2). This may be due to substantial dust particles and strong northwesterly winds diluting local anthropogenic pollutants (Wang et al., 2012).

Thermo-derived carbonaceous components provide valuable clues concerning potential sources of organic aerosols (Chow et al., 2004). In general, OC1 primarily has a biomass burning source; OC2, OC3, and OC4 are associated with coal combustion; EC1 is associated with gasoline vehicle exhaust; and EC2 and EC3 may be related to diesel vehicle emissions (Chow et al., 2004; Cao et al., 2005). The concentrations of these carbonaceous components at the three sites are summarized in Table S1 and their mass fractions are shown in Fig. S6. The average concentration of OC1 in non-dust samples from Zhangbei (0.76 $\pm$ 1.00 μg m^{-3}) was 2–4 times that at the other sites, indicating the potential influence of biomass burning. The high OC2, OC3, OC4, and EC1 concentrations at Jinan indicate that coal combustion and traffic emissions are important sources. Miyazaki et al. (2007) investigated thermograms derived from standard organic compounds of different molecular weights and found that compounds evolved at higher temperatures, such as OC3 and OC4, are generally related to higher molecular weight compounds; while those evolved at lower temperatures (e.g., OC1) are associated with lower molecular weight and more volatile compounds. The concentrations of highly refractory compounds (OC3 and OC4) increased significantly at Erenhot during dust events, accounting for 61.1% of the total carbonaceous components, while the contribution of low and medium refractory compound groups (OC1 and OC2) decreased to ~5%. Similar variations were observed at Zhangbei but were not obvious at Jinan due to the reduced dust masses. These results imply that the high molecular weight compounds are significant contributors to organics in dust aerosols.

3.2. Light-absorbing properties of WS-BrC

The UV–Vis absorption coefficients of WSOC at the three sampling sites exhibited strong wavelength dependence (increasing sharply towards shorter wavelengths) with different temporal variations (Fig. 3). The average Abs$_{365}$ values in non-dust periods at Jinan (8.35 $\pm$ 2.77 Mm^{-1}) and Zhangbei (6.38 $\pm$ 2.99 Mm^{-1}) were 3–4 times those at Erenhot (1.88 $\pm$ 0.60 Mm^{-1}). During dust periods, Abs$_{365}$ values were elevated at Erenhot (average of 3.51 $\pm$ 1.10 Mm^{-1}), while reduced at Zhangbei and Jinan. The robust linear correlations between Abs$_{365}$ values and EC concentrations during non-dust periods at Zhangbei ($r = 0.89$, $p < 0.001$) and Jinan ($r = 0.75$, $p < 0.001$) (Table S2) indicate that the sources of WS-BrC were

associated with combustion emissions. Coals and biomass fuels are two major sources of energy in China, which contribute significantly to atmospheric BrC (Yan et al., 2018; Li et al., 2019). Jinan is an important industrial city in northern China with high coal consumption, where coal-fired power plants contributing ~10% of total electricity production (Yang et al., 2012). In rural and suburban areas of northern China, bulk coal, wheat straw, and corn stalks are cheap and easy-access fuels and are used extensively for domestic heating (generally from November to late April) and cooking (Shen et al., 2007). Significant positive correlations between Abs$_{365}$ values and SO$_4^{2-}$ concentrations were found for the three sites (Table S2), likely associated with the widespread use of coal in northern China, although the low EC and SO$_4^{2-}$ concentrations at Erenhot indicate it is less influenced by anthropogenic activities (Table 1). Abs$_{365}$ values are also strongly correlated ($r = 0.82$, $p < 0.001$) with nss-ndust-K$^+$ concentrations (fraction of K$^+$ that not related to sea salt and mineral dust, a reliable tracer for biomass burning; Text S3) for Zhangbei samples, indicating that biomass burning is the primary combustion source of WS-BrC there. At the Jinan site, NO$_3^-$ was the most abundant anion with an average concentration of 20.21 $\pm$ 13.89 μg m^{-3}, contributing 28.7% of the total measured ions (Fig. S7). Abs$_{365}$ values were strongly correlated with NO$_3^-$ concentrations ($r = 0.83$, $p < 0.001$), with NO$_3^-$ being a product of NO$_x$ oxidation, indicating the important contribution of vehicle exhausts there (Pio et al., 2007).

The AAE has been widely used in characterizing atmospheric BrC from specific sources and chemical processes (Chen and Bond, 2010; Hecobian et al., 2010). For aqueous extracts of aerosol samples derived from biomass burning, AAE values are usually around 6–9 (Hecobian et al., 2010; Fan et al., 2016; Park and Yu, 2016), and higher for coal burning samples up to 13 (Li et al., 2019). Bones et al. (2010) found that AAE values decreased during the atmospheric aging process, from 7 for freshly formed to 4.7 for aged biogenic secondary organic aerosol (SOA). Here, the average AAE value at Erenhot (5.04 $\pm$ 0.35) was comparable with that measured previously in the high-altitude Himalayas (4.9 $\pm$ 0.7; Kirillova et al., 2016). The highest average AAE value of the three sites was found at Zhangbei (5.58 $\pm$ 0.50), with a range of 4.56–6.89, covering the range of various types of biomass fuel burning (Table S3). The high OC/EC (4.59 $\pm$ 1.48) and nss-ndust-K$^+$/EC (0.21 $\pm$ 0.10) ratios at Zhangbei also indicate the impact of biomass burning (Srinivas and Sarin, 2014; Dasari et al., 2019). In contrast, AAE values at Jinan varied only slightly (4.73–6.09) with a lower average of 5.37 $\pm$ 0.26, indicating that sources of WS-BrC changed little during the study; the average value is consistent with those observed in urban areas such as New Delhi, India (5.1 $\pm$ 2.0; Kirillova et al., 2014) and Xi'an, China (5.11 $\pm$ 0.53; Li et al., 2020).

The MAE is a key parameter in characterizing the light-absorption capacity of BrC. In this study, MAE$_{365}$ values decreased in the series of Zhangbei (1.32 $\pm$ 0.34 m^2 g^{-1}) > Jinan (1.00 $\pm$ 0.23 m^2 g^{-1}) > Erenhot (0.84 $\pm$ 0.30 m^2 g^{-1}). The average value for Zhangbei is in the range of those from rice- and corn-straw burning (1.24–1.56; Fan et al., 2016). while the average for Erenhot is comparable with those reported by Wu et al. (2019a) for TSP samples collected on the southeastern Tibetan Plateau in winter (0.86 $\pm$ 0.17 m^2 g^{-1}). The MAE$_{365}$ value at Jinan is consistent with the results reported in urban areas of Nanjing (1.0 $\pm$ 0.2 m^2 g^{-1}; Liu et al., 2019) and Xi'an (1.00 $\pm$ 0.18 m^2 g^{-1}; Li et al., 2020), China, but lower than those in New Delhi, India (1.6 $\pm$ 0.5 m^2 g^{-1}; Kirillova et al., 2014) and Beijing, China (1.54 $\pm$ 0.16 m^2 g^{-1}; Yan et al., 2015). When dust events occurred at Zhangbei and Jinan, the AAE and MAE$_{365}$ values decreased due to the dilution effect of the dust plumes; whereas the increased values at Erenhot indicate that the optical properties of WS-BrC there are strongly affected by frequent dust events (Table S3). The ratios of MAE$_{250}$ to MAE$_{365}$ (E$_2$/E$_3$) were 4.90 $\pm$ 0.53, 5.99 $\pm$ 0.93, and 5.33 $\pm$ 0.27 for non-dust samples from Erenhot, Zhangbei, and Jinan, respectively. Previous studies have reported that the E$_2$/E$_3$ ratio is negatively correlated with the average molecular weight and total aromaticity of organics
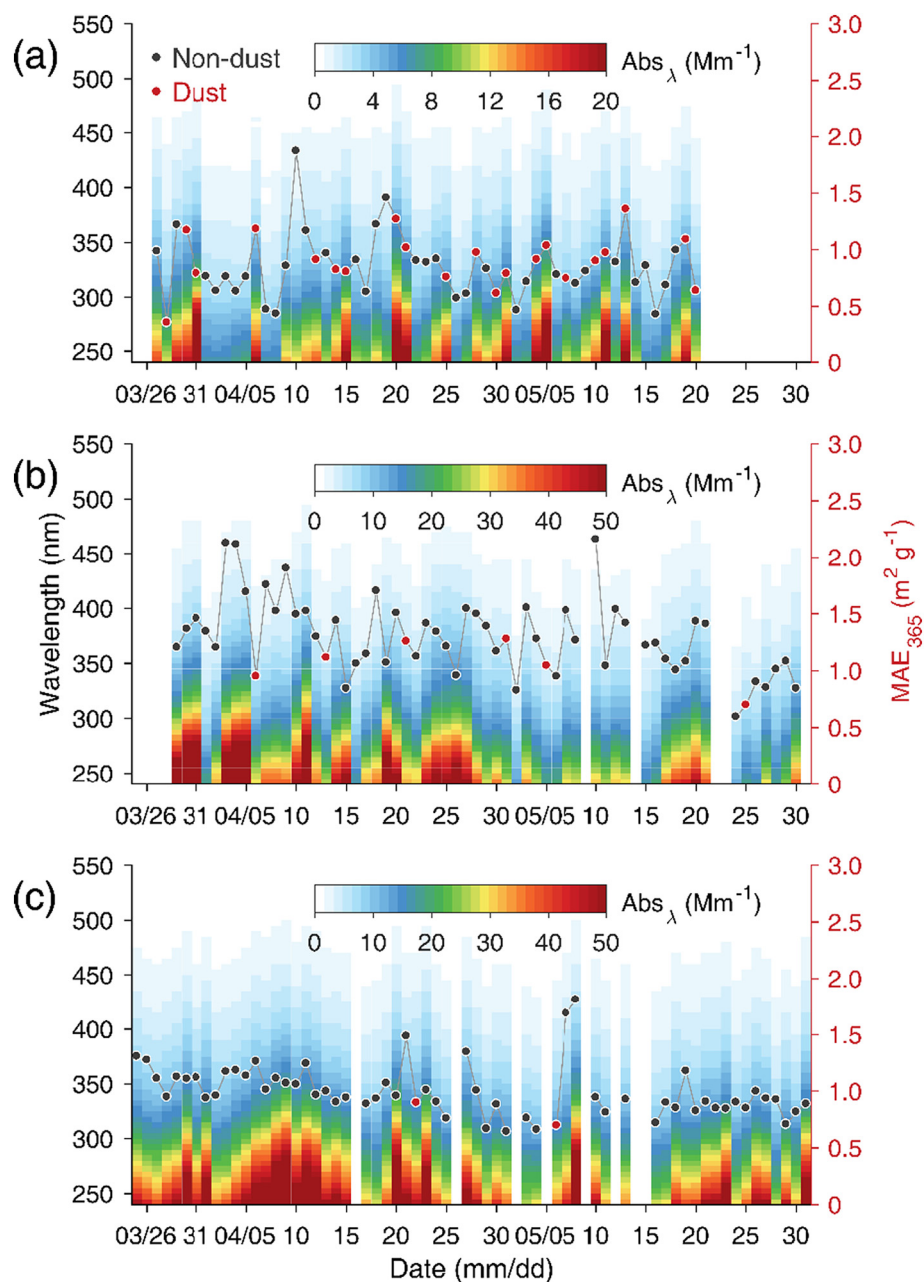
Fig. 3. Temporal variations in light absorption coefficients (Abs_λ, Mm^{-1}) of WSOC at wavelength range of 240–550 nm (left y-axis) at (a) Erenhot, (b) Zhangbei, and (c) Jinan sites. MAE_{365} values are marked as dots (right y-axis). Black and red dots represent the non-dust and dust samples, respectively.

(Peuravuori and Pihlaja, 1997; Duarte et al., 2005). The substantially higher E_2/E_3 ratio at Zhangbei implies that WS-BrC of the rural area has lower molecular weight and aromaticity relative to those in remote and urban areas. Conversely, the lowest E_2/E_3 ratio for dust samples from Erenhot (5.12 ± 0.46), indicates that WS-BrC from desert regions has a high molecular weight and aromaticity, consistent with characteristics of thermal-derived carbonaceous compounds (Section 3.1).

3.3. Fluorescence properties of WS-BrC

3.3.1. Characteristics of PARAFAC components

Four independent fluorescent components (abbreviated C1–C4) were resolved from EEMs using the PARAFAC model; their profiles are shown in Fig. 4. Based on the comparison of excitation/emission (Ex/

Em) peak positions of the PARAFAC-derived components with typical fluorescent spectra reported in previous studies, C1 and C2 (both with $\lambda_{Em} > 380$ nm) were identified as humic-like substances (HULIS) commonly detected in aerosols and rainwater (Kieber et al., 2006; Chen et al., 2016b). Two apparent peaks were observed in C1 (Fig. 4a): a strong peak at <240/393 nm (Ex/Em) and a weak peak at 315/393 nm. C1 is usually recognized as less oxygenated HULIS, as reported in urban aerosols (Chen et al., 2016a; Wang et al., 2020) and seasonal snow samples (Zhou et al., 2019), and are related to anthropogenic or terrestrial sources. Previous studies have shown that the fluorescence peak position of organics was influenced strongly by their molecular size and chemical structure (Duarte et al., 2004; Stubbins et al., 2014). The appearance of emission peaks at longer wavelengths is generally attributed to higher molecular weight, higher conjugation, and highly
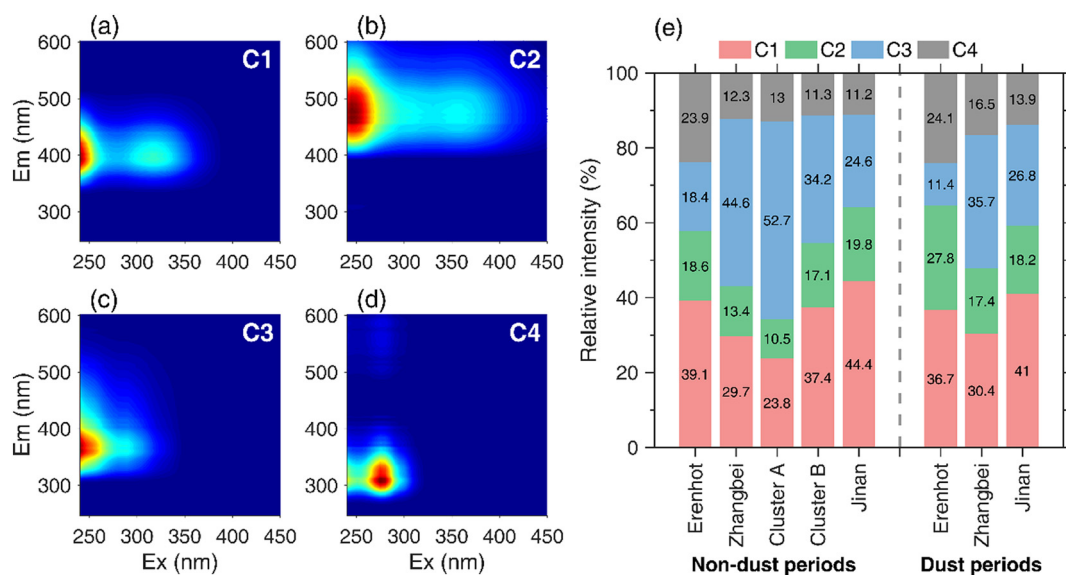
Fig. 4. (a–d) The four fluorescent components (C1–C4) identified by PARAFAC analysis; (e) relative abundances of fluorescent components during dust and non-dust periods at the three sampling sites.

functionalized compounds (Kieber et al., 2006). Compared to C1, the primary (secondary) peak of C2 appeared at longer Ex/Em of 245 (360)/476 nm with an excitation tail extending to ~440 nm (Fig. 4b), which is classified as highly-oxygenated HULIS (Chen et al., 2016b). Similar fluorophores were identified in aerosol samples from urban areas of Godavari, Nepal (Wu et al., 2019b) and Xi'an, China (Chen et al., 2020), most likely derived from terrestrial and dust sources.

C3 is dominated by a strong peak at <240/361 nm (Ex/Em) with a small shoulder at around 290/361 nm (Fig. 4c). Emission peaks at shorter wavelengths (<380 nm) are generally associated with protein-like organic matter (PLOM) such as tryptophan and tyrosine, with lower aromaticity and smaller molecular sizes (Cory and McKnight, 2005). However, recent studies have found that some non-nitrogen-containing species with optically active functional groups (e.g., phenols) also exhibit fluorescence in the PLOM region (Rosario-Ortiz and Korak, 2017; Fan et al., 2020). Phenolic compounds are important BrC chromophores with high absorption efficiencies (Moschos et al., 2018), emitted directly from biomass burning as incomplete pyrolysis products of lignin and cellulose (Fan et al., 2016; Lavi et al., 2017). Tang et al. (2020) found that C3-like fluorophores were abundant (~30% of total fluorescence intensity) in water-soluble extracts of biomass burning smoke, while did not appear in vehicle or cooking emissions.

C4 exhibit a strong peak at 275/311 nm (Fig. 4d), with a possible additional peak appeared at Ex <240 nm (not shown here for clarity, due to the limited range of analyses), closely matching the typical profile of tyrosine (Pohlker et al., 2012). Yan and Kim (2017) resolved a similar component in rainwater in Seoul, Korea, and found that the intensities of C4-like fluorophores were significantly correlated with concentrations of total hydrolysable tyrosine. C4 is consistently associated with microbial activity (Birdwell and Valsaraj, 2010; Zhou et al., 2019). Similar fluorophores are also enriched (~19% of total fluorescence intensity) in marine aerosols, attributed mainly to marine biological materials (Chen et al., 2016b).

3.3.2. Variations in fluorescent components

The intensities of individual fluorescent components relative to total fluorescence intensity are commonly applied in tracking the origin of chromophores (Murphy et al., 2013; Wang et al., 2020). The relative contributions of the C1–C4 components at the different sampling sites, under dust and non-dust conditions, are shown in Fig. 4e. Overall, the

two HULIS components (C1 and C2) dominate the total fluorescence during non-dust periods at Erenhot and Jinan with average contributions of 57.7% and 64.2%, respectively, consistent with previous results for aerosol samples in urban and remote areas. For example, HULIS accounted for ~70% of total fluorescence intensity in the urban area of Granada, Spain (Mladenov et al., 2011a) and ~ 66% at the remote and high Colorado Rocky Mountains, USA (Xie et al., 2016). Here, C1 is a significant contributor to fluorophores not only in the polluted Jinan site (44.4%) but also in the relatively clean Erenhot site (39.1%). During dust events, the average relative intensity of C2 increased significantly from 18.6% to 27.8% ($p < 0.001$, two-tailed t-test) at Erenhot and slightly at Zhangbei from 13.4% to 17.4%, suggesting a link with highly-oxygenated HULIS of terrestrial origin such as desert dust. However, the relative intensity of C2 decreased slightly, from 19.8% to 18.2%, during dust periods at Jinan, possible due to either (1) when dust plumes arrive at Jinan after long-range transport they are too weak to modify the local OA composition; or (2) abundant air pollutants of strong oxidation capacity (e.g., NO_x, O_3, and OH radicals) in urban areas may contribute to the formation of highly-oxygenated organic species (Tong et al., 2019), leading to a higher C2 fraction than that of dust organics. Among four fluorescent components, C3 was the largest contributor to total fluorescence intensity during non-dust periods at Zhangbei, with an average relative intensity of 44.6% ± 11.2%, almost twice those at Erenhot (18.3% ± 7.9%) and Jinan (24.6% ± 5.2%). However, this proportion dropped rapidly to 35.7% ± 10.7% during events at Zhangbei. The average contribution of C4 during non-dust periods at Erenhot (23.9%) was twice those at Zhangbei and Jinan (12.3% and 11.2%, respectively), and it also increased during dust events at the three sites (Fig. 4e). Our earlier study revealed that the richness and diversity of bioaerosols were substantially higher in dust aerosols from the Gobi Desert (Tang et al., 2018). Microbial activity is significant in the aerosols from desert regions, even impacting the composition of aerosols in downwind regions.

The relative intensities of fluorophores varied considerably during non-dust periods at Zhangbei. For example, the C1 contribution ranged from 12.7% to 47.6% and C3 from 19.9% to 68.6%. A hierarchical cluster analysis was performed to further classify non-dust samples from Zhangbei ($n = 53$) based on the relative intensities of PARAFAC-derived components. The dendrogram in Fig. S8 indicates that the samples can be divided into two clusters, Clusters A and B. Most (25 of 30) samples in Cluster A were collected in March and April 2016, while

most (19 of 23) of those in Cluster B were collected in May 2016. In addition, the relative intensities of C3 are negatively correlated with daily average ambient temperature ($r = 0.78$, $p < 0.001$; Fig. S9), with the temperature increasing from the sampling time of Cluster A (6.7 ± 3.9 °C) to Cluster B (14.9 ± 3.6 °C). Considering the significant positive correlation ($r = 0.47$, $p < 0.01$) between the relative intensities of C3 and the mass fractions of nss-ndust-K$^+$ for Cluster A samples (Table S4), the high contributions of C3 (maximum: 68.6%) may be attributable to heavy emissions from biomass fuel combustion for household heating. Dark smoke emission from nearby residential houses was often observed under low-temperature conditions (see Fig. S10), providing further evidence for this inference. We therefore conclude that the most likely source of C3 is the local biomass burning in residential areas around the sampling site in Zhangbei.

The most pronounced feature of Cluster A samples is that C3 dominated the total fluorescence (52.7% on average), much more than those in Cluster B (34.2%); while C1 and C2 contributed less to Cluster A (23.8% and 10.5%, respectively) than Cluster B (37.4% and 17.1%, respectively). There are two possible reasons for the highly variable WS-BrC compositions recorded during non-dust periods at Zhangbei. First, correlation coefficients between relative intensities of fluorescent components and mass fractions of inorganic ions for the two clusters are considerably different (Table S4), possibly indicating that emission sources of WS-BrC differed between sampling periods at Zhangbei. Second, Fan et al. (2020) reported more C1-like HULIS but fewer C3-like PLOM fluorescent components in aged biomass burning smoke than in fresh smoke, which was explained by the conversion of susceptible PLOM of relatively low molecular weight, probably phenolic compounds, to more oxygenated species of larger molecular weight and more complex structures (e.g., HULIS) through atmospheric photooxidation (Matos et al., 2015). In this study, the average F_{max}(C1) to F_{max}(C3) ratios were 0.47 for Cluster A samples and 1.17 for Cluster B samples, possibly due to the chemical transformation of WS-BrC. The higher contributions of HULIS, especially less-oxygenated HULIS (i.e., C1), in Cluster B may therefore also be attributed to the photoaging of phenolic compounds in fresh biomass burning aerosols (Fan et al., 2020; Bianco et al., 2014).

3.3.3. Fluorescence-derived indices

Fluorescence-derived indicators provide insights into sources and chemical properties of chromophores and have been widely applied in studies of aquatic and terrestrial environments (Zsolnay et al., 1999; Cory and McKnight, 2005; Huguet et al., 2009). Three widely used fluorescence-derived indices are summarized in Table S5. The fluorescence index (FI) is the ratio of fluorescence intensity at 370/470 nm (Ex/Em) to that at 370/520 nm (Cory and McKnight, 2005). Previous

studies have shown that the FI value has a strong negative relationship with the aromatic carbon content of dissolved organic matter (McKnight et al., 2001), and can also reflect the extent of photobleaching of atmospheric WSOC (Xie et al., 2016). Here, the relatively higher average FI value was found at Zhangbei (1.75 ± 0.08), while lower at Jinan (1.64 ± 0.05) and Erenhot (1.62 ± 0.09), suggesting lower WSOC aromaticity for Zhangbei samples, consistent with E_2/E_3 results (Section 3.2). The average FI value for Cluster A samples of Zhangbei (1.79 ± 0.06) was higher than that for Cluster B (1.69 ± 0.05) (Fig. 5a), indicating a lower degree of photobleaching for Cluster A than Cluster B samples (Xie et al., 2016). The average FI value for dust samples from Erenhot was 1.58 ± 0.04, consistent with previous results for dust plumes from the Sahara Desert (1.48–1.59; Mladenov et al., 2011a).

The biological index (BIX, aka "freshness index") is defined as the ratio of the fluorescence intensity at Ex/Em = 310/380 nm to that at 310/430 nm (Huguet et al., 2009). A higher BIX value generally indicates a large contribution of freshly-released organics, while lower values are associated with organics with higher degrees of aging/decomposition or terrestrial input (Huguet et al., 2009; Lee et al., 2013). Compared to non-dust periods, the relatively low BIX values (0.71 ± 0.08) for dust samples from Erenhot are attributed to organics from terrestrial sources (e.g., dust or soil) with high degrees of aging/decomposition. Jinan values for non-dust samples (0.95 ± 0.09) are within the range reported for cloud water samples collected at the Mt. Tai, China (0.73–1.27; Zhao et al., 2019) but higher than those from biogenic SOA (mean: 0.6; Lee et al., 2013). Chen et al. (2016b) found that BIX values of WSOC are positively correlated with the signal intensity of $C_2H_4O_2^+$ ions, an indicator of biomass burning organic aerosol. Zhangbei Cluster A samples presented much higher BIX values (1.40 ± 0.15) than those of Cluster B (1.07 ± 0.12), possibly reflecting the potentially important contribution of freshly-emitted OA from biomass burning.

Recent studies of atmospheric OA have shown that humification index (HIX) values increase significantly during the atmospheric aging process reflecting a higher degree of condensation (i.e., lower H/C ratios) (Lee et al., 2013; Fan et al., 2020). However, HIX values for WSOC in ambient aerosol samples are lower than those in aquatic and terrestrial dissolved organic matter (Mladenov et al., 2011a; Fu et al., 2015; Xie et al., 2016). Therefore, the commonly used fluorescence-derived indices may need to be redefined due to the diverse sources of aerosols and their complex aging processes in the atmosphere (Wu et al., 2021). Considering the high contribution of tyrosine-like substance (C4) in dust samples from Erenhot, we adjusted the calculation of HIX (refer to as "HIX$_{adj}$", hereinafter) to better reflect the difference between the three sites; a detailed explanation is given in Text S4 and Fig. S11. The average HIX$_{adj}$ value exhibited a decreasing trend of
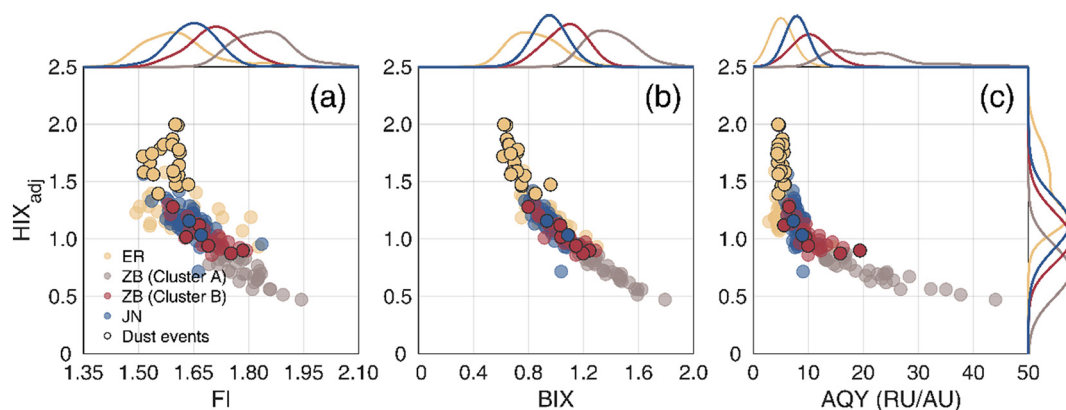
Fig. 5. Scatter plots of HIX$_{adj}$ versus (a) FI, (b) BIX, and (c) AQY for the samples of Erenhot (ER), Zhangbei (ZB), and Jinan (JN) sites. Markers with black edges indicate dust samples. Marginal plots show probability density distributions for each variable on the corresponding axis.

Erenhot (1.22 ± 0.41) > Jinan (1.14 ± 0.13) > Zhangbei (0.85 ± 0.19). The highest average HIX$_{adj}$ value (1.68 ± 0.17) was found in dust samples from Erenhot, indicating that WSOC from desert regions has a higher degree of aging/oxidation. Fan et al. (2020) reported that HIX values of three types of biomass burning smoke increased from ~1 to 2–4.5 during the O$_3$ aging process, possibly associated with the formation of polyhydroxylated aromatic compounds through the oxidation of phenolic compounds. The average HIX$_{adj}$ value of Cluster A samples of Zhangbei (0.71 ± 0.11) is significantly ($p <$ 0.001; two-tailed t-test) lower than that of Cluster B (1.02 ± 0.11), again indicating an increased contribution of fresh OA from biomass burning rather than aged OA in Cluster A samples.

3.3.4. Fluorescence energy parameters

Fluorescence quantum yield is an important factor in the assessment of climatic effects of BrC (Aiona et al., 2018). The Stokes shift provides information about the energy loss from the molecular vibration relaxation of fluorescent molecules, and is defined as the difference between the peak emission wavelength and the corresponding excitation wavelength (nm) (Lee et al., 2013; Phillips and Smith, 2015). These parameters have rarely been reported in previous studies (Aiona et al., 2018; Harrison et al., 2020; Yang et al., 2020). The large Stokes shift for dust samples from Erenhot (mean: 104 nm) indicates large π-conjugated organic molecules (Xiao et al., 2018), consistent with indications of fluorescence-derived indices. Spectral valleys at around 280 nm in all dust samples (Fig. 6) are attributed to the abundance of PLOM fluorophores (i.e., C4). However, no significant difference was observed in average Stokes shift values between dust and non-dust samples from Jinan, indicating the marginal influence of long-range dust plumes transport.

Dust samples from Erenhot have lower AQY values than non-dust samples (Table S5). The variation in AQY values for Jinan samples (Fig. 6f) were similar to those for aged anthropogenic SOA (i.e., benzene, toluene, and p-xylene) (Aiona et al., 2018), indicating the possible influence of anthropogenic sources at the Jinan site. The average integral AQY value for Cluster A samples of Zhangbei was about twice that for Cluster B. This, together with the significantly higher relative contribution of C3 to Cluster A samples, suggests that the higher AQY values for Cluster A samples may be ascribed mainly to C3 fluorophores of higher fluorescence efficiency. Furthermore, the AQY value decreased monotonically with increasing HIX$_{adj}$ value (Fig. 5c), indicating that the fluorescence intensity of OA may be efficiently quenched by aging processes (i.e., solar irradiation and various

oxidants) (Aiona et al., 2018; Fan et al., 2019). Freshly emitted biomass burning OA (Cluster A) of relatively low aromaticity and molecular weight (reflected by higher BIX and FI, lower HIX and Stokes shift values) may thus have a higher fluorescence efficiency than aged biomass burning (Cluster B), urban (Jinan), and dust-sourced (Erenhot) OA of higher aromaticity and molecular weight.

3.4. Radiative effects

The radiative effect of WS-BrC was evaluated from its fractional solar absorption relative to that of EC (Section 2.4.4). For non-dust samples from Erenhot, the integrated solar radiation absorbed by WS-BrC in the range 300–1000 nm ($f_{300–1000}$) was equivalent to 8.6% ± 8.8% of that absorbed by BC (Table S6), similar to that in the high Arctic (13% ± 7.0%; Yue et al., 2019). Relatively low values were observed at Zhangbei and Jinan (3.4% ± 0.9% and 2.3% ± 1.4%, respectively), lower than those recorded in previous studies in urban areas such as Beijing (5.7% ± 2.5% in summer and 10.7% ± 3.0% in winter; Yan et al., 2015) and New Delhi (6 ± 3% in winter; Kirillova et al., 2014). However, when considering the UV range ($f_{300–400}$) only, this fraction increased to 31.3% ± 31.4%, 13.9% ± 3.9%, and 9.2% ± 6.3% for Erenhot, Zhangbei, and Jinan, respectively. This indicates that the light-absorbing effect of WS-BrC should not be ignored, especially at shorter wavelengths and in remote areas. Higher fractions were obtained in dust samples from Zhangbei and Jinan (69.2% ± 23.0% and 16.5% ± 6.3% for $f_{300–400}$, 17.6% ± 5.9% and 4.3% ± 1.4% for $f_{300–1000}$, respectively), possibly due to dispersal of local pollutions such as BC by strong winds and the input of organic matter carried by dust particles (Wang et al., 2013). Because almost all samples collected during dust periods at Erenhot had extremely low EC values (even below the detection limit, see Section 3.1), these samples were not available for calculation of the fraction f. We thus assumed that WS-BrC is the main light-absorbing carbonaceous species (rather than EC) during the dust events. It should be noted that a significant fraction of BrC is water-insoluble (Liu et al., 2013), so the total radiative absorbance contribution of BrC may be higher than our estimate.

The wavelength-dependent absorption SFE of WS-BrC is shown in Fig. 7 for the different cases. The integrated mean SFE$_{abs}$ values for 300–1000 nm (SFE$_{abs-300-1000}$) were 2.70 ± 0.97, 4.08 ± 1.05, and 3.33 ± 0.75 W g^{-1} for non-dust samples from Erenhot, Zhangbei, and Jinan, respectively. The average SFE$_{abs-300-1000}$ value for Cluster A samples from Zhangbei was 18% higher than those of Cluster B, indicating higher radiation forcing efficiency for freshly than aged biomass
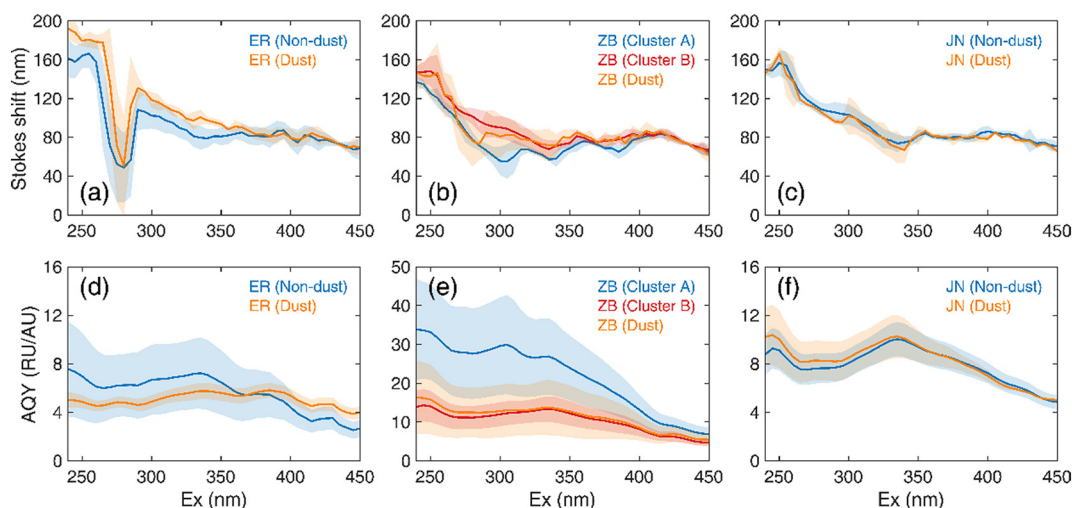
Fig. 6. The variations in Stokes shift (a–c) and AQY (d–f) against the excitation wavelength at the three sites. Solid lines and shaded areas represent the averages and one-time t standard errors, respectively.
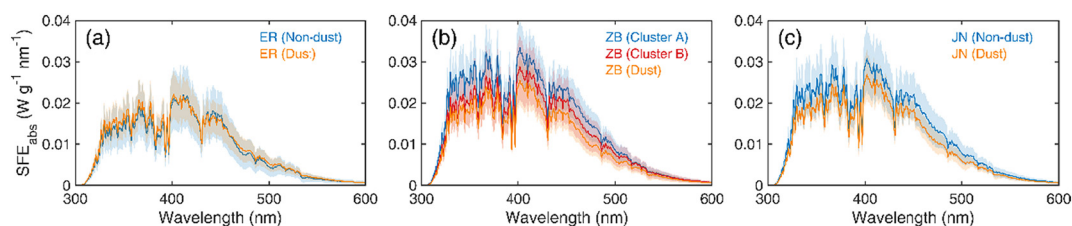
Fig. 7. Direct forcing efficiency of WS-BrC for the three sites.

burning OA at Zhangbei. The value for Cluster A samples is about half that of laboratory biofuel combustion samples (7.7–8.3 W g^{-1}, in 280–700 nm; Lei et al., 2018), but twice that of samples influenced by biomass burning in the Indo-Gangetic Plain (2.5 ± 1.9 W g^{-1}, in 300–700 nm; Bikkina and Sarin, 2019). During dust events, $SFE_{abs\_300-1000}$ values increased slightly at Erenhot (to 9.1%) but decreased substantially at Zhangbei and Jinan (to 21.1% and 22.5%, respectively), suggesting a lower radiation forcing efficiency for dust-derived WS-BrC than those from biomass burning and fuel/coal combustion. These results emphasize that WS-BrC plays an important role in the radiative balance of the Earth climate system, and potentially its atmospheric photochemistry.

4. Summary and conclusions

Optical properties, chemical compositions, and potential sources of extracted WSOC from three sites—Erenhot, Zhangbei, and Jinan—along the transport pathway of Asian dust were investigated. Atmospheric WSOC concentrations averaged 2.31 ± 0.50 μg m^{-3} at Erenhot, 4.92 ± 2.23 μg m^{-3} at Zhangbei, and 8.40 ± 2.39 μg m^{-3} at Jinan. The WSOC concentrations of the dust samples from Erenhot (3.91 ± 0.96 μg m^{-3}) were almost twice those of non-dust periods. Average MAE_{365} values displayed a trend of Zhangbei (1.32 ± 0.34 m^2 g^{-1}) > Jinan (1.00 ± 0.23 m^2 g^{-1}) > Erenhot (0.84 ± 0.30 m^2 g^{-1}). During dust events, AAE and MAE_{365} values decreased at Zhangbei and Jinan due to the dilution effect of strong winds, while values at Erenhot increased due to the input of dust-derived organics of high molecular weight. Correlation analysis of Abs_{365} and major inorganic ions (nss-ndust-K^+, SO_4^{2-}, and NO_3^-) indicated potential sources of WS-BrC. Strong correlations between Abs_{365} and SO_4^{2-} were found at all three sites, suggesting a widespread coal combustion source. Erenhot suffered frequent and severe dust storms but was less affected by anthropogenic activities. The strong correlation between Abs_{365} and nss-ndust-K^+ at Zhangbei indicates the impact of local biomass burning, while the correlation of Abs_{365} with NO_3^- at Jinan indicates more vehicle exhaust impact.

EEM spectroscopy combined with PARAFAC analysis identified four independent fluorescent components, including two humic-like (C1 and C2) and two protein-like (C3 and C4) substances. C1 and C2 represent less- and highly-oxygenated humic-like substances (HULIS), respectively, which together account for ~64% of total fluorescence in the highly polluted urban Jinan site. During dust events, the relative contribution of C2 increased significantly, due mainly to highly-oxygenated HULIS compounds from desert regions. The most likely C3 source is biomass burning-derived phenolic compounds, which represented a considerable proportion (~45%) of total fluorescence at the rural Zhangbei site. C4 is associated with biogenic substances (e.g., microbes and plant debris) from desert regions, which contributed more (~24%) in Erenhot samples.

Non-dust samples from Zhangbei can be divided into two clusters (Clusters A and B) based on hierarchical cluster analysis. The fluorescent component in Cluster A was dominated by C3 (~53%), which were mainly affected by freshly biomass burning aerosol; while Cluster B samples may undergo photooxidation or other aging processes, leading

to a much lower C3 fraction (~34%). We speculate that the susceptible C3 components are transformed into humic-like fluorophores through atmospheric aging processes, providing an additional pathway for the formation of atmospheric HULIS (Fan et al., 2020). Compared to other sites, Cluster A samples of Zhangbei have higher AQY, FI, and BIX values, but lower HIX and Stokes shift values, indicating that biomass burning-derived WS-BrC at Zhangbei has higher fluorescence efficiency but lower molecular weight, average aromaticity, and degree of aging than aged biomass burning (Cluster B), urban (Jinan), and dust-sourced (Erenhot) OA.

During non-dust periods, the relative absorption of WS-BrC compared to EC at 300–1000 nm ($f_{300-1000}$) was 8.6%, 3.4%, and 2.3% at Erenhot, Zhangbei, and Jinan, with $f_{300-400}$ values of 31.3%, 13.9%, and 9.2%; and corresponding broadband integrated mean $SFE_{abs\_300-1000}$ values of 2.70 ± 0.97, 4.08 ± 1.05, and 3.33 ± 0.75 W g^{-1}, respectively. The light-absorbing effect of WS-BrC is notable, especially in remote areas and at shorter wavelengths.

This study presents a comprehensive overview of WSOC extracted from three types of aerosol samples (i.e., remote, rural, and urban) in northern China, and can improve understanding of the optical properties, sources, and climatic effects of WS-BrC. Our main conclusions are as follows. (1) Dust deposition can be an important source of WSOC in remote regions such as Erenhot; (2) dust particles from the Gobi Desert carry abundant biogenic substances, and can be transported over long distances, affecting downwind areas; (3) biomass burning-derived WS-BrC at the rural Zhangbei site has higher absorption and fluorescence efficiency than that from the urban Jinan and remote Erenhot sites; (4) the light-absorbing effect of WS-BrC should not be ignored in radiative forcing models, especially at shorter wavelengths.

CRediT authorship contribution statement

Hui Wen: Conceptualization, Methodology, Writing – original draft, Visualization. **Yue Zhou:** Conceptualization, Writing – review & editing. **Xuanye Xu:** Data curation. **Tianshuang Wang:** Data curation. **Quanliang Chen:** Methodology. **Qingcai Chen:** Methodology. **Weijun Li:** Methodology. **Zhe Wang:** Methodology. **Zhongwei Huang:** Investigation, Methodology. **Tian Zhou:** Investigation, Methodology. **Jinsen Shi:** Investigation, Methodology. **Jianrong Bi:** Investigation, Methodology. **Mingxia Ji:** Investigation, Methodology. **Xin Wang:** Funding acquisition, Writing – review & editing.

Declaration of competing interest

The authors declare that they have no conflict of interest.

Acknowledgments

Appendix A. Supplementary data

Supplementary data to this article can be found online at https://doi.org/10.1016/j.scitotenv.2021.147971.

References

Aiona, P.K., Lee, H.J., Leslie, R., Lin, P., Laskin, A., Laskin, J., Nizkorodov, S.A., 2017. Photochemistry of products of the aqueous reaction of methylglyoxal with ammonium sulfate. ACS Earth Space Chem. 1, 522–532.

Aiona, P.K., Luek, J.L., Timko, S.A., Powers, L.C., Gonsior, M., Nizkorodov, S.A., 2018. Effect of photolysis on absorption and fluorescence spectra of light-absorbing secondary organic aerosols. ACS Earth Space Chem. 2, 235–245.

Alexander, J.M., Grassian, V.H., Young, M.A., Kleiber, P.D., 2015. Optical properties of selected components of mineral dust aerosol processed with organic acids and humic material. J. Geophys. Res.-Atmos. 120, 2437–2452.

Andreae, M.O., Gelencsér, A., 2006. Black carbon or brown carbon? The nature of light-absorbing carbonaceous aerosols, Atmos. Chem. Phys. 6, 3131–3148.

Bianco, A., Minella, M., De Laurentiis, E., Maurino, V., Minero, C., Vione, D., 2014. Photochemical generation of photoactive compounds with fulvic-like and humic-like fluorescence in aqueous solution. Chemosphere 111, 529–536.

Bikkina, S., Sarin, M., 2019. Brown carbon in the continental outflow to the North Indian Ocean. Environ Sci Process Impacts 21, 970–987.

Birdwell, J.E., Engel, A.S., 2010. Characterization of dissolved organic matter in cave and spring waters using UV-Vis absorbance and fluorescence spectroscopy, Org. Geochem. 41, 270–280.

Birdwell, J.E., Valsaraj, K.T., 2010. Characterization of dissolved organic matter in fogwater by excitation-emission matrix fluorescence spectroscopy, Atmos. Environ. 44, 3246–3253.

Bond, T.C., Bergstrom, R.W., 2006. Light absorption by carbonaceous particles: an investigative review, Aerosol Sci. Tech. 40, 27–67.

Bond, T.C., Doherty, S.J., Fahey, D.W., Forster, P.M., Berntsen, T., DeAngelo, B.J., Flanner, M.G., Ghan, S., Karcher, B., Koch, D., Kinne, S., Kondo, Y., Quinn, P.K., Sarofim, M.C., Schultz, M.G., Schulz, M., Venkataraman, C., Zhang, H., Zhang, S., Bellouin, N., Guttikunda, S.K., Hopke, P.K., Jacobson, M.Z., Kaiser, J.W., Klimont, Z., Lohmann, U., Schwarz, J.P., Shindell, D., Storelvmo, T., Warren, S.G., Zender, C.S., 2013. Bounding the role of black carbon in the climate system: a scientific assessment. J. Geophys. Res.-Atmos. 118, 5380–5552.

Bones, D. L., Henricksen, D. K., Mang, S. A., Gonsior, M., Bateman, A. P., Nguyen, T. B., Cooper, W. J., and Nizkorodov, S. A.: Appearance of strong absorbers and fluorophores in limonene-O-3 secondary organic aerosol due to NH4+-mediated chemical aging over long time scales, J. Geophys. Res.-Atmos., 115, Artn D05203, 2010.

Bosch, C., Andersson, A., Kirillova, E.N., Budhavant, K., Tiwari, S., Praveen, P.S., Russell, L.M., Beres, N.D., Ramanathan, V., Gustafsson, O., 2014. Source-diagnostic dual-isotope composition and optical properties of water-soluble organic carbon and elemental carbon in the South Asian outflow intercepted over the Indian Ocean. J. Geophys. Res.-Atmos. 119, 11743–11759.

Cao, J.J., Wu, F., Chow, J.C., Lee, S.C., Li, Y., Chen, S.W., An, Z.S., Fung, K.K., Watson, J.G., Zhu, C.S., Liu, S.X., 2005. Characterization and source apportionment of atmospheric organic and elemental carbon during fall and winter of 2003 in Xi'an, China, Atmos. Chem. Phys. 5, 3127–3137.

Chen, Q., Wang, M., Wang, Y., Zhang, L., Li, Y., Han, Y., 2019. Oxidative potential of water-soluble matter associated with chromophoric substances in PM2.5 over. Sci. Technol, Xi'an, China, Environ.

Chen, Q., Li, J., Hua, X., Jiang, X., Mu, Z., Wang, M., Wang, J., Shan, M., Yang, X., Fan, X., Song, J., Wang, Y., Guan, D., Du, L., 2020. Identification of species and sources of atmospheric chromophores by fluorescence excitation-emission matrix with parallel factor analysis, Sci. Total Environ. 718, 137322.

Chen, Q.C., Ikemori, F., Mochida, M., 2016a. Light absorption and excitation-emission fluorescence of urban organic aerosol components and their relationship to chemical structure, Environ. Sci. Technol. 50, 10859–10868.

Chen, Q.C., Miyazaki, Y., Kawamura, K., Matsumoto, K., Coburn, S., Volkamer, R., Iwamoto, Y., Kagami, S., Deng, Y.G., Ogawa, S., Ramasamy, S., Kato, S., Ida, A., Kajii, Y., Mochida, M., 2016b. Characterization of chromophoric water-soluble organic matter in urban, forest, and marine aerosols by HR-ToF-AMS analysis and excitation emission matrix spectroscopy, Environ. Sci. Technol. 50, 10351–10360.

Chen, S.Y., Huang, J.P., Li, J.X., Jia, R., Jiang, N.X., Kang, L.T., Ma, X.J., Xie, T.T., 2017. Comparison of dust emissions, transport, and deposition between the Taklimakan Desert and Gobi Desert from 2007 to 2011, Sci. China Earth Sci. 60, 1338–1355.

Chen, Y., Bond, T.C., 2010. Light absorption by organic carbon from wood combustion, Atmos. Chem. Phys. 10, 1773–1787.

Cheng, Y., He, K.B., Zheng, M., Duan, F.K., Du, Z.Y., Ma, Y.L., Tan, J.H., Yang, F.M., Liu, J.M., Zhang, X.L., Weber, R.J., Bergin, M.H., Russell, A.G., 2011. Mass absorption efficiency of elemental carbon and water-soluble organic carbon in Beijing, China, Atmos. Chem. Phys. 11, 11497–11510.

Chow, J.C., Watson, J.G., 2002. PM2.5 carbonate concentrations at regionally representative Interagency Monitoring of Protected Visual Environment sites. J. Geophys. Res.-Atmos. 107, 9.

Chow, J.C., Watson, J.G., Kuhns, H., Etyemezian, V., Lowenthal, D.H., Crow, D., Kohl, S.D., Engelbrecht, J.P., Green, M.C., 2004. Source profiles for industrial, mobile, and area sources in the Big Bend Regional Aerosol Visibility and Observational study. Chemosphere 54, 185–208.

Chow, J.C., Watson, J.G., Chen, L.W.A., Chang, M.C.O., Robinson, N.F., Trimble, D., Kohl, S., 2007. The IMPROVE-A temperature protocol for thermal/optical carbon analysis: maintaining consistency with a long-term database. J. Air Waste Manage. Assoc. 57, 1014–1023.

Coble, P.G., 1996. Characterization of marine and terrestrial DOM in seawater using excitation emission matrix spectroscopy. Mar. Chem. 51, 325–346.

Cory, R.M., McKnight, D.M., 2005. Fluorescence spectroscopy reveals ubiquitous presence of oxidized and reduced quinones in dissolved organic matter, Environ. Sci. Technol. 39, 8142–8149.

Dasari, S., Andersson, A., Bikkina, S., Holmstrand, H., Budhavant, K., Satheesh, S., Asmi, E., Kesti, J., Backman, J., Salam, A., Bisht, D. S., Tiwari, S., Hameed, Z., and Gustafsson, O.: Photochemical degradation affects the light absorption of water-soluble brown carbon in the South Asian outflow, Sci. Adv., 5, ARTN eaau8066, 2019.

Decesari, S., Facchini, M. C., Matta, E., Mircea, M., Fuzzi, S., Chughtai, A. R., and Smith, D. M.: Water soluble organic compounds formed by oxidation of soot, Atmos. Environ., 36, 1827–1832, PII S1352-2310(02)00141-3, 2002.

Duarte, R.M.B.O., Pio, C.A., Duarte, A.C., 2004. Synchronous scan and excitation-emission matrix fluorescence spectroscopy of water-soluble organic compounds in atmospheric aerosols. J. Atmos. Chem. 48, 157–171.

Duarte, R.M.B.O., Pio, C.A., Duarte, A.C., 2005. Spectroscopic study of the water-soluble organic matter isolated from atmospheric aerosols collected under different atmospheric conditions, Anal. Chim. Acta 530, 7–14.

Duce, R.A., Unni, C.K., Ray, B.J., Prospero, J.M., Merrill, J.T., 1980. Long-range atmospheric transport of soil dust from Asia to the Tropical North Pacific: temporal variability. Science 209, 1522–1524.

Fan, X.J., Wei, S.Y., Zhu, M.B., Song, J.Z., Peng, P.A., 2016. Comprehensive characterization of humic-like substances in smoke PM2.5 emitted from the combustion of biomass materials and fossil fuels, Atmos. Chem. Phys. 16, 13321–13340.

Fan, X.J., Yu, X.F., Wang, Y., Xiao, X., Li, F.Y., Xie, Y., Wei, S.Y., Song, J.Z., Peng, P.A., 2019. The aging behaviors of chromophoric biomass burning brown carbon during dark aqueous hydroxyl radical oxidation processes in laboratory studies, Atmos. Environ. 205, 9–18.

Fan, X.J., Cao, T., Yu, X.F., Wang, Y., Xiao, X., Li, F.Y., Xie, Y., Ji, W.C., Song, J.Z., Peng, P.A., 2020. The evolutionary behavior of chromophoric brown carbon during ozone aging of fine particles from biomass burning, Atmos. Chem. Phys. 20, 4593–4605.

Feng, Y., Ramanathan, V., Kotamarthi, V.R., 2013. Brown carbon: a significant atmospheric absorber of solar radiation?, Atmos. Chem. Phys. 13, 8607–8621.

Fu, P. Q., Kawamura, K., Chen, J., Qin, M. Y., Ren, L. J., Sun, Y. L., Wang, Z. F., Barrie, L. A., Tachibana, E., Ding, A. J., and Yamashita, Y.: Fluorescent water-soluble organic aerosols in the High Arctic atmosphere, Sci. Rep.-UK, 5, Artn 9845, 2015.

Garrison, V.H., Shinn, E.A., Foreman, W.T., Griffin, D.W., Holmes, C.W., Kellogg, C.A., Majewski, M.S., Richardson, L.L., Ritchie, K.B., Smith, G.W., 2003. African and Asian dust: from desert soils to coral reefs. Bioscience 53, 469–480.

Gustafsson, O., Krusa, M., Zencak, Z., Sheesley, R.J., Granat, L., Engstrom, E., Praveen, P.S., Rao, P.S.P., Leck, C., Rodhe, H., 2009. Brown clouds over South Asia: biomass or fossil fuel combustion? Science 323, 495–498.

Harrison, A.W., Waterson, A.M., De Bruyn, W.J., 2020. Spectroscopic and photochemical properties of secondary brown carbon from aqueous reactions of methylglyoxal. ACS Earth Space Chem. 4, 762–773.

Hecobian, A., Zhang, X., Zheng, M., Frank, N., Edgerton, E.S., Weber, R.J., 2010. Water-soluble organic aerosol material and the light-absorption characteristics of aqueous extracts measured over the southeastern United States, Atmos. Chem. Phys. 10, 5965–5977.

Huang, J., Minnis, P., Chen, B., Huang, Z., Liu, Z., Zhao, Q., Yi, Y., Ayers, J.K., 2008. Long-range transport and vertical structure of Asian dust from CALIPSO and surface measurements during PACDEX. J. Geophys. Res.-Atmos. 113.

Huang, J., Wang, T., Wang, W., Li, Z., Yan, H., 2014. Climate effects of dust aerosols over East Asian arid and semiarid regions. J. Geophys. Res. Atmos. 119, 2.

Huang, Z. W., Huang, J. P., Hayasaka, T., Wang, S. S., Zhou, T., and Jin, H. C.: Short-cut transport path for Asian dust directly to the Arctic: a case study, Environ. Res. Lett., 10, Artn 114018, 2015.

Husar, R. B., Tratt, D. M., Schichtel, B. A., Falke, S. R., Li, F., Jaffe, D., Gasso, S., Gill, T., Laulainen, N. S., Lu, F., Reheis, M. C., Chun, Y., Westphal, D., Holben, B. N., Gueymard, C., McKendry, I., Kuring, N., Feldman, G. C., McClain, C., Frouin, R. J., Merrill, J., DuBois, D., Vignola, F., Murayama, T., Nickovic, S., Wilson, W. E., Sassen, K., Sugimoto, N., and Malm, W.C. Asian dust events of April 1998, J. Geophys. Res.-Atmos., 106, 18317–18330, 2001.

IPCC: Climate Change, 2013. In: Stocker, T.F., Qin, D., Plattner, G.-K., Tignor, M., Allen, S.K., Boschung, J., Nauels, A., Xia, Y., Bex, V., Midgley, P.M. (Eds.), The Physical Science Basis. Contribution of Working Group I to the Fifth Assessment Report of the Intergovernmental Panel on Climate Change. Cambridge University Press, Cambridge, United Kingdom and New York, NY, USA 1535 pp., 2013.

Kieber, R. J., Whitehead, R. F., Reid, S. N., Willey, J. D., and Seaton, P. J.: Chromophoric dissolved organic matter (CDOM) in rainwater, southeastern North Carolina, USA, J. Atmos. Chem., 54, 21–41, 2006.

Kim, H., Kim, J.Y., Jin, H.C., Lee, J.Y., Lee, S.P., 2016. Seasonal variations in the light-absorbing properties of water-soluble and insoluble organic aerosols in Seoul, Korea, Atmos. Environ. 129, 234–242.

Kirillova, E.N., Andersson, A., Tiwari, S., Srivastava, A.K., Bisht, D.S., Gustafsson, O., 2014. Water-soluble organic carbon aerosols during a full New Delhi winter: isotope-based source apportionment and optical properties. J. Geophys. Res.-Atmos. 119, 3476–3485.

Kirillova, E.N., Marinoni, A., Bonasoni, P., Vuillermoz, E., Facchini, M.C., Fuzzi, S., Decesari, S., 2016. Light absorption properties of brown carbon in the high Himalayas. J. Geophys. Res.-Atmos. 121, 9621–9639.

Kothawala, D.N., Murphy, K.R., Stedmon, C.A., Weyhenmeyer, G.A., Tranvik, L.J., 2013. Inner filter correction of dissolved organic matter fluorescence, Limnol. Oceanogr.-Meth. 11, 616–630.

Kumagai, K., Iijima, A., Tago, H., Tomioka, A., Kozawa, K., Sakamoto, K., 2009. Seasonal characteristics of water-soluble organic carbon in atmospheric particles in the inland Kanto plain, Japan, Atmos. Environ. 43, 3345–3351.

Laskin, A., Laskin, J., Nizkorodov, S.A., 2015. Chemistry of atmospheric brown carbon. Chem. Rev. 115, 4335–4382.

Lavi, A., Lin, P., Bhaduri, B., Carmieli, R., Laskin, A., Rudich, Y., 2017. Characterization of light-absorbing oligomers from reactions of phenolic compounds and Fe(III). ACS Earth Space Chem. 1, 637–646.

Lee, H.J., Laskin, A., Laskin, J., Nizkorodov, S.A., 2013. Excitation-emission spectra and fluorescence quantum yields for fresh and aged biogenic secondary organic aerosols. Environ. Sci. Technol. 47, 5763–5770.

Lee, H.J., Aiona, P.K., Laskin, A., Laskin, J., Nizkorodov, S.A., 2014. Effect of solar radiation on the optical properties and molecular composition of laboratory proxies of atmospheric brown carbon, Environ. Sci. Technol. 48, 10217–10226.

Lei, Y., Shen, Z., Zhang, T., Zhang, Q., Wang, Q., Sun, J., Gong, X., Cao, J., Xu, H., Liu, S., Yang, L., 2018. Optical source profiles of brown carbon in size-resolved particulate matter from typical domestic biofuel burning over Guanzhong Plain, China. Sci. Total Environ. 622–623, 244–251.

Li, J., Zhang, Q., Wang, G., Li, J., Wu, C., Liu, L., Wang, J., Jiang, W., Li, L., Ho, K.F., Cao, J., 2020. Optical properties and molecular compositions of water-soluble and water-insoluble brown carbon (BrC) aerosols in northwest China, Atmos. Chem. Phys. 20, 4889–4904.

Li, M., Fan, X., Zhu, M., Zou, C., Song, J., Wei, S., Jia, W., Peng, P. a, 2019. Abundance and light absorption properties of brown carbon emitted from residential coal combustion in China, Environ. Sci. Technol. 53, 595–603.

Lin, P., Liu, J.M., Shilling, J.E., Kathmann, S.M., Laskin, J., Laskin, A., 2015. Molecular characterization of brown carbon (BrC) chromophores in secondary organic aerosol generated from photo-oxidation of toluene. Phys. Chem. Chem. Phys. 17, 23312–23325.

Liu, J., Bergin, M., Guo, H., King, L., Kotra, N., Edgerton, E., Weber, R.J., 2013. Size-resolved measurements of brown carbon in water and methanol extracts and estimates of their contribution to ambient fine-particle light absorption, Atmos. Chem. Phys. 13, 12389–12404.

Liu, X., Zhang, Y.-L., Peng, Y., Xu, L., Zhu, C., Cao, F., Zhai, X., Haque, M.M., Yang, C., Chang, Y., Huang, T., Xu, Z., Bao, M., Zhang, W., Fan, M., Lee, X., 2019. Chemical and optical properties of carbonaceous aerosols in Nanjing, eastern China: regionally transported biomass burning contribution, Atmos. Chem. Phys. 19, 11213–11233.

Matos, J.T.V., Freire, S.M.S.C., Duarte, R.M.B.O., Duarte, A.C., 2015. Natural organic matter in urban aerosols: comparison between water and alkaline soluble components using excitation-emission matrix fluorescence spectroscopy and multiway data analysis, Atmos. Environ. 102, 1–10.

McKnight, D.M., Boyer, E.W., Westerhoff, P.K., Doran, P.T., Kulbe, T., Andersen, D.T., 2001. Spectrofluorometric characterization of dissolved organic matter for indication of precursor organic material and aromaticity, Limnol. Oceanogr. 46, 38–48.

Miyazaki, Y., Kondo, Y., Han, S., Koike, M., Kodama, D., Komazaki, Y., Tanimoto, H., Matsueda, H., 2007. Chemical characteristics of water-soluble organic carbon in the Asian outflow. J. Geophys. Res.-Atmos. 112, Artn D22s30.

Mladenov, N., Alados-Arboledas, L., Olmo, F.J., Lyamani, H., Delgado, A., Molina, A., Reche, I., 2011a. Applications of optical spectroscopy and stable isotope analyses to organic aerosol source discrimination in an urban area, Atmos. Environ. 45, 1960–1969.

Mladenov, N., Sommaruga, R., Morales-Baquero, R., Laurion, I., Camarero, L., Dieguez, M. C., Camacho, A., Delgado, A., Torres, O., Chen, Z., Felip, M., and Reche, I.: Dust inputs and bacteria influence dissolved organic matter in clear alpine lakes, Nat. Commun., 2, ARTN 405, 2011b.

Moschos, V., Kumar, N.K., Daellenbach, K.R., Baltensperger, U., Prevot, A.S.H., El Haddad, I., 2018. Source apportionment of brown carbon absorption by coupling ultraviolet-visible spectroscopy with aerosol mass spectrometry, environ. Sci. Tech. Let. 5, 302–308.

Murphy, K.R., Stedmon, C.A., Graeber, D., Bro, R., 2013. Fluorescence spectroscopy and multi-way techniques. PARAFAC, Anal Methods-Uk 5, 6557–6566.

Nishita-Hara, C., Hirabayashi, M., Hara, K., Yamazaki, A., Hayashi, M., 2019. Dithiothreitol-measured oxidative potential of size-segregated particulate matter in Fukuoka, Japan: effects of Asian dust events. GeoHealth 3, 160–173.

Ohno, T., Amirbahman, A., Bro, R., 2008. Parallel factor analysis of excitation-emission matrix fluorescence spectra of water soluble soil organic matter as basis for the determination of conditional metal binding parameters, Environ. Sci. Technol. 42, 186–192.

Park, S.S., Yu, J., 2016. Chemical and light absorption properties of humic-like substances from biomass burning emissions under controlled combustion experiments, Atmos. Environ. 136, 114–122.

Pathak, R.K., Wang, T., Ho, K.F., Lee, S.C., 2011. Characteristics of summertime PM2.5 organic and elemental carbon in four major Chinese cities: implications of high acidity for water-soluble organic carbon (WSOC). Atmos. Environ. 45, 318–325.

Peuravuori, J., Pihlaja, K., 1997. Molecular size distribution and spectroscopic properties of aquatic humic substances, Anal. Chim. Acta 337, 133–149.

Phillips, S.M., Smith, G.D., 2015. Further evidence for charge transfer complexes in brown carbon aerosols from excitation-emission matrix fluorescence spectroscopy. J. Phys. Chem. A 119, 4545–4551.

Pio, C.A., Legrand, M., Oliveira, T., Afonso, J., Santos, C., Caseiro, A., Fialho, P., Barata, F., Puxbaum, H., Sanchez-Ochoa, A., Kasper-Giebl, A., Gelencser, A., Preunkert, S., Schock, M., 2007. Climatology of aerosol composition (organic versus inorganic) at nonurban sites on a west-east transect across Europe. J. Geophys. Res.-Atmos. 112.

Pohlker, C., Huffman, J.A., Poschl, U., 2012. Autofluorescence of atmospheric bioaerosols - fluorescent biomolecules and potential interferences, Atmos. Meas. Tech. 5, 37–71.

Qian, W.H., Quan, L.S., Shi, S.Y., 2002. Variations of the dust storm in China and its climatic control. J. Clim. 15, 1216–1229.

Ram, K., Sarin, M.M., Tripathi, S.N., 2012. Temporal trends in atmospheric PM2.5, PM10, elemental carbon, organic carbon, water-soluble organic carbon, and optical properties: impact of biomass burning emissions in the Indo-Gangetic Plain. Environ. Sci. Technol. 46, 686–695.

Rosario-Ortiz, F.L., Korak, J.A., 2017. Oversimplification of dissolved organic matter fluorescence analysis: potential pitfalls of current methods. Environ. Sci. Technol. 51, 759–761.

Saleh, R., 2020. From measurements to models: toward accurate representation of brown carbon in climate calculations. Curr. Pollut. Rep. 6, 90–104.

Saleh, R., Hennigan, C.J., McMeeking, G.R., Chuang, W.K., Robinson, E.S., Coe, H., Donahue, N.M., Robinson, A.L., 2013. Absorptivity of brown carbon in fresh and photochemically aged biomass-burning emissions, Atmos. Chem. Phys. 13, 7683–7693.

Shen, Z. X., Cao, J. J., Arimoto, R., Zhang, R. J., Jie, D. M., Liu, S. X., and Zhu, C.S. Chemical composition and source characterization of spring aerosol over Horqin sand land in northeastern China, J. Geophys. Res.-Atmos., 112, Artn D14315, 2007.

Simoneit, B.R.T., Kobayashi, M., Mochida, M., Kawamura, K., Lee, M., Lim, H.J., Turpin, B.J., Komazaki, Y., 2004. Composition and major sources of organic compounds of aerosol particulate matter sampled during the ACE-Asia campaign. J. Geophys. Res.-Atmos. 109, Artn D19s10.

Slikboer, S., Grandy, L., Blair, S.L., Nizkorodov, S.A., Smith, R.W., Al-Abadleh, H., 2015. A.: formation of light absorbing soluble secondary organics and insoluble polymeric particles from the dark reaction of catechol and guaiacol with Fe(III). Environ. Sci. Technol. 49, 7793–7801.

Srinivas, B., Sarin, M.M., 2014. Brown carbon in atmospheric outflow from the Indo-Gangetic Plain: mass absorption efficiency and temporal variability, Atmos. Environ. 89, 835–843.

Stedmon, C.A., Markager, S., 2005. Resolving the variability in dissolved organic matter fluorescence in a temperate estuary and its catchment using PARAFAC analysis. Limnol. Oceanogr. 50, 686–697.

Stubbins, A., Lapierre, J.F., Berggren, M., Prairie, Y.T., Dittmar, T., del Giorgio, P.A., 2014. What's in an EEM? Molecular signatures associated with dissolved organic fluorescence in Boreal Canada, Environ. Sci. Technol. 48, 10598–10606.

Tang, J., Li, J., Su, T., Han, Y., Mo, Y., Jiang, H., Cui, M., Jiang, B., Chen, Y., Tang, J., Song, J., Peng, P., Zhang, G., 2020. Molecular compositions and optical properties of dissolved brown carbon in biomass burning, coal combustion, and vehicle emission aerosols illuminated by excitation–emission matrix spectroscopy and Fourier transform ion cyclotron resonance mass spectrometry analysis, Atmos. Chem. Phys. 20, 2513–2532.

Tang, K., Huang, Z.W., Huang, J.P., Maki, T., Zhang, S., Shimizu, A., Ma, X.J., Shi, J.S., Bi, J.R., Zhou, T., Wang, G.Y., Zhang, L., 2018. Characterization of atmospheric bioaerosols along the transport pathway of Asian dust during the Dust-Bioaerosol 2016 Campaign, Atmos. Chem. Phys. 18, 7131–7148.

Tang, M., Cziczo, D.J., Grassian, V.H., 2016. Interactions of water with mineral dust aerosol: water adsorption, hygroscopicity, cloud condensation, and ice nucleation. Chem. Rev. 116, 4205–4259.

Tobo, Y., Zhang, D.Z., Matsuki, A., Iwasaka, Y., 2010. Asian dust particles converted into aqueous droplets under remote marine atmospheric conditions, P. Natl. Acad. Sci. USA 107, 17905–17910.

Tong, H.J., Zhang, Y., Filippi, A., Wang, T., Li, C.P., Liu, F.B., Leppla, D., Kourtchev, I., Wang, K., Keskinen, H.M., Levula, J.T., Arangio, A.M., Shen, F.X., Ditas, F., Martin, S.T., Artaxo, P., Godoi, R.H.M., Yamamoto, C.I., de Souza, R.A.F., Huang, R.J., Berkemeier, T., Wang, Y.S., Su, H., Cheng, Y.F., Pope, F.D., Fu, P.Q., Yao, M.S., Pohlker, C., Petaja, T., Kulmala, M., Andreae, M.O., Shiraiwa, M., Poschl, U., Hoffmann, T., Kalberer, M., 2019. Radical formation by fine particulate matter associated with highly oxygenated molecules, Environ. Sci. Technol. 53, 12506–12518.

Uno, I., Eguchi, K., Yumimoto, K., Takemura, T., Shimizu, A., Uematsu, M., Liu, Z.Y., Wang, Z.F., Hara, Y., Sugimoto, N., 2009. Asian dust transported one full circuit around the globe. Nat. Geosci. 2, 557–560.

Wang, G. H., Kawamura, K., and Lee, M.: Comparison of organic compositions in dust storm and normal aerosol samples collected at Gosan, Jeju Island, during spring 2005, Atmos. Environ., 43, 219–227, 2009a.

Wang, G. H., Kawamura, K., Umemoto, N., Xie, M. J., Hu, S. Y., and Wang, Z.F. Water-soluble organic compounds in PM2.5 and size-segregated aerosols over Mount Tai in North China Plain, J. Geophys. Res.-Atmos., 114, Artn D19208, 2009b.

Wang, G. H., Li, J. J., Cheng, C. L., Zhou, B. H., Xie, M. J., Hu, S. Y., Meng, J. J., Sun, T., Ren, Y. Q., Cao, J. J., Liu, S. X., Zhang, T., and Zhao, Z. Z. Observation of atmospheric aerosols at Mt. Hua and Mt. Tai in central and east China during spring 2009-Part 2: impact of dust storm on organic aerosol composition and size distribution, Atmos. Chem. Phys., 12, 4065–4080, 2012.

Wang, G.H., Zhou, B.H., Cheng, C.L., Cao, J.J., Li, J.J., Meng, J.J., Tao, J., Zhang, R.J., Fu, P.Q., 2013. Impact of Gobi desert dust on aerosol chemistry of Xi'an, inland China during spring 2009: differences in composition and size distribution between the urban ground surface and the mountain atmosphere, Atmos. Chem. Phys. 13, 819–835.

Wang, G.H., Cheng, C.L., Huang, Y., Tao, J., Ren, Y.Q., Wu, F., Meng, J.J., Li, J.J., Cheng, Y.T., Cao, J.J., Liu, S.X., Zhang, T., Zhang, R., Chen, Y.B., 2014. Evolution of aerosol chemistry in Xi'an, inland China, during the dust storm period of 2013-Part 1: sources, chemical forms and formation mechanisms of nitrate and sulfate. Atmos. Chem. Phys. 14, 11571–11585.

Wang, H.B., Zhang, L.M., Huo, T.T., Wang, B., Yang, F.M., Chen, Y., Tian, M., Qiao, B.Q., Peng, C., 2020. Application of parallel factor analysis model to decompose excitation-emission matrix fluorescence spectra for characterizing sources of water-soluble brown carbon in PM2.5. Atmos. Environ. 223, 117192.

Wu, G., Wan, X., Ram, K., Li, P., Liu, B., Yin, Y., Fu, P., Loewen, M., Gao, S., Kang, S., Kawamura, K., Wang, Y., and Cong, Z.: Light absorption, fluorescence properties and sources of brown carbon aerosols in the Southeast Tibetan Plateau, Environ. Pollut., 113616–113616, 2019a.

Wu, G.M., Ram, K., Fu, P.Q., Wang, W., Zhang, Y.L., Liu, X.Y., Stone, E.A., Pradhan, B.B., Dangol, P.M., Panday, A.K., Wan, X., Bai, Z.P., Kang, S.C., Zhang, Q.G., Cong, Z.Y., 2019b. Water-soluble brown carbon in atmospheric aerosols from Godavari (Nepal), a regional representative of South Asia, Environ. Sci. Technol. 53, 3471–3479.

Wu, G.M., Fu, P.Q., Ram, K., Song, J.Z., Chen, Q.C., Kawamura, K., Wan, X., Kang, S.C., Wang, X.P., Laskin, A., Cong, Z.Y., 2021. Fluorescence characteristics of water-soluble organic carbon in atmospheric aerosol. Environ. Pollut. 268, 115906.

Xiao, K., Shen, Y.X., Sun, J.Y., Liang, S., Fan, H.J., Tan, J.H., Wang, X.M., Huang, X., Waite, T.D., 2018. Correlating fluorescence spectral properties with DOM molecular weight and size distribution in wastewater treatment systems, Environ. Sci.-Wat. Res. 4, 1933–1943.

Xie, M.J., Mladenov, N., Williams, M.W., Neff, J.C., Wasswa, J., Hannigan, M.P., 2016. Water soluble organic aerosols in the Colorado Rocky Mountains, USA: composition, sources and optical properties, Sci. Rep.-UK 6.

Yan, C.Q., Zheng, M., Sullivan, A.P., Bosch, C., Desyaterik, Y., Andersson, A., Li, X.Y., Guo, X.S., Zhou, T., Gustafsson, O., Collett, J.L., 2015. Chemical characteristics and light-absorbing property of water-soluble organic carbon in Beijing: biomass burning contributions, Atmos. Environ. 121, 4–12.

Yan, C.Q., Zheng, M., Sullivan, A.P., Shen, G.F., Chen, Y.J., Wang, S.X., Zhao, B., Cai, S.Y., Desyaterik, Y., Li, X.Y., Zhou, T., Gustafsson, O., Collett, J.L., 2018. Residential coal combustion as a source of Levoglucosan in China. Environ. Sci. Technol. 52, 1665–1674.

Yan, G., Kim, G., 2017. Speciation and sources of brown carbon in precipitation at Seoul, Korea: insights from excitation-emission matrix spectroscopy and carbon isotopic analysis. Environ. Sci. Technol. 51, 11580–11587.

Yang, L.X., Zhou, X.H., Wang, Z., Zhou, Y., Cheng, S.H., Xu, P.J., Gao, X.M., Nie, W., Wang, X.F., Wang, W.X., 2012. Airborne fine particulate pollution in Jinan, China: concentrations, chemical compositions and influence on visibility impairment, Atmos. Environ. 55, 506–514.

Yang, Y., Qin, J., Qi, T., Zhou, X., Chen, R., Tan, J., Xiao, K., Ji, D., He, K., Chen, X., 2020. Fluorescence characteristics of particulate water-soluble organic compounds emitted from coal-fired boilers, Atmos. Environ. 223, 117297.

Yue, S.Y., Bikkina, S., Gao, M., Barrie, L., Kawamura, K., Fu, P.Q., 2019. Sources and radiative absorption of water-soluble brown carbon in the high Arctic atmosphere. Geophys. Res. Lett. 46, 14881–14891.

Zhang, X.L., Lin, Y.H., Surratt, J.D., Weber, R.J., 2013. Sources, composition and absorption angstrom exponent of light-absorbing organic components in aerosol extracts from the Los Angeles Basin, Environ. Sci. Technol. 47, 3685–3693.

Zhao, W.Y., Fu, P.Q., Yue, S.Y., Li, L.J., Xie, Q.R., Zhu, C., Wei, L.F., Ren, H., Li, P., Li, W.J., Sun, Y.L., Wang, Z.F., Kawamura, K., Chen, J.M., 2019. Excitation-emission matrix fluorescence, molecular characterization and compound-specific stable carbon isotopic composition of dissolved organic matter in cloud water over Mt. Tai, Atmos. Environ. 213, 608–619.

Zhou, Y., Wen, H., Liu, J., Pu, W., Chen, Q.C., Wang, X., 2019. The optical characteristics and sources of chromophoric dissolved organic matter (CDOM) in seasonal snow of northwestern China. Cryosphere 13, 157–175.

Zsolnay, A., Baigar, E., Jimenez, M., Steinweg, B., Saccomandi, F., 1999. Differentiating with fluorescence spectroscopy the sources of dissolved organic matter in soils subjected to drying. Chemosphere 38, 45–50.